Venus Atmospheric, Ionospheric, Surface and Interplanetary Radio-Wave Propagation Studies with the VeRA Radio-Science Experiment

B. Häusler[1], M. Pätzold[2], G.L. Tyler[3], V.J.-P. Barriot[7], M.K. Bird[4], V. Dehant[6]; D. Hinson[3], R.A. Simpson[3], R.A. Treumann[5], W. Eidel[1], R. Mattei[1], P. Rosenblatt[6], S. Remus[1], J. Selle[1] & S. Tellmann[2]

[1]*Institut für Raumfahrttechnik, Universität der Bundeswehr München, D-85577 Neubiberg, Germany*
Email: bernd.haeusler@unibw-muenchen.de
[2]*Institut für Geophysik und Meteorologie, Universität zu Köln, D-50923 Köln, Germany*
[3]*Space, Telecommunications and Radioscience Laboratory, Department of Electrical Engineering, Stanford University, Stanford, CA 95305, USA*
[4]*Argelander Institut für Astronomie, Universität Bonn, D-53121 Bonn, Germany*
[5]*Max-Planck-Institut für extraterrestrische Physik, D-85748 Garching, Germany*
[6]*Observatoire Royal de Belgique, B-1180 Bruxelles, Belgium*
[7]*Observatoire Midi-Pyrénées, F-31400 Toulouse, France*

The Venus Express Radio-Science Experiment (VeRa) is using radio signals at X- and S-band (3.5 cm and 13 cm wavelengths, respectively) to probe the Venus surface, neutral atmosphere, ionosphere and gravity field, and the interplanetary medium. An ultrastable oscillator (USO) is providing a high-quality onboard reference frequency source; instrumentation on Earth is sampling amplitude, phase, propagation time and polarisation of the received signals. Simultaneous coherent measurements at the two wavelengths allow separation of dispersive media effects from classical Doppler shift. The execution of a radio-science experiment involves the precise interaction of many complex spaceborne and ground-based systems. The quality of the measurements depend critically not only on the noise performance of the USO, the quality of the radio link and the performance of the ground station, but also on the precision of the timing, ephemeris data, orbit prediction and the attitude-control manoeuvres that are needed to perform the experiments and to extract the data.

1. Introduction

The Venus Express Radio-Science Experiment (VeRa) applies radio-science techniques to the study of atmospheric, ionospheric, gravity and surface questions at Venus, and to the study of the solar corona and wind. There is a long history of such experiments (Howard et al., 1974; 1992; Eshleman et al., 1977; Tyler, 1987; Steffes et al., 1994; Tyler et al., 1992; 2000; 2001; Bird et al., 1994; 1997; Pätzold et al., 1995, 2006). A set of companion investigations on Mars Express was decribed by Pätzold et al. (2004).

Radio-science investigations fall into three broad categories of experimentation and observation. First, for the study of planetary atmospheres and ionospheres, the spacecraft must be 'occulted' so that the gas or plasma lies between the radio source and receiver. In a typical occultation experiment conducted with an orbiter, the spacecraft sequentially passes behind the ionosphere, the neutral atmosphere and finally the planetary disc as seen from the tracking station, and then reemerges in the reverse sequence. During an occultation event, the media of interest (atmosphere and ionosphere) are 'sensed'

VeRa's science objectives include:

Determination of neutral atmospheric structure from the cloud deck (~40 km) to 100 km altitude and derivation of vertical profiles of neutral mass density, temperature and pressure as a function of local time and season. The results should also reveal the vertical structure of localised buoyancy waves, and the presence and properties of planetary waves.

Study of the sulphuric acid vapour absorbing layer in the atmosphere by signal intensity variations, as a tracer for atmospheric motions. Scintillation effects caused by diffraction of the radio wave within the atmosphere can also provide information on small-scale turbulence effects.

Investigation of ionospheric structure from about 80 km to the ionopause (< 600 km), to study the interaction between solar wind plasma and the atmosphere and ionosphere of Venus.

Observation of forward-scattered surface echoes obliquely reflected from high-elevation targets with anomalous radar properties (such as Maxwell Montes). More generally, such bistatic radar measurements provide information on roughness and density of the surface material on scales of cm to m.

Study of gravity anomalies, to provide insights into the properties of the crust and lithosphere.

Measurement of the Doppler shift, the propagation time and the Doppler noise, especially during superior and inferior conjunction, allows investigation of dynamical processes in the solar corona and solar wind.

by their effects on the radio signals (Fjeldbo & Eshleman, 1969; Fjeldbo et al., 1971; Eshleman, 1973). In the case of coherent dual-frequency transmission, this experiment allows the separation of non-dispersive and dispersive media effects; it becomes possible to distinguish between neutral atmospheres and ionised media. This technique is able to study not only planetary ionospheres but also solar corona and solar wind effects.

Second, oblique-incidence scattering investigations using propagation paths from a spacecraft via a planetary or satellite surface to an Earth station can be used to explore the surface properties through study of the microwave scattering function. Such investigations are referred to as 'bistatic radar' since the transmitter and receiver are separated by significant angular distances or ranges. For Venus, the detailed relationship between surface emissivity, reflectivity and altitude is still a major unresolved issue.

Third, in contrast to occultation experiments, which sense the effect of the medium along a path between two known points, gravity experiments are based on determining the motion of the spacecraft in response to the variations in mass-distribution within a planet or its satellites. For Venus, the spherical harmonic gravity field was determined to degree and order 180 by Barriot et al. (1998) and Konopliv et al. (1999), but questions concerning the properties of the crust and lithosphere below special target areas remain open.

In all cases, a radio-science experiment relies on the extreme stability of the frequencies employed and measured. Performing a radio-science experiment requires the precise interaction of many complex spaceborne and ground-based systems, an equally precise numerical analysis and simulation to separate predicted effects of orbit, tropospheric and ionospheric path delays, planetary motion and relativity from the observed effects. This paper therefore not only presents instrumental details but also describes the typical interaction of many physical and technical disciplines needed for the success of the experiment.

VeRa is the first radio science experiment carried out at Venus using an ultrastable reference frequency source aboard the satellite.

2. Science Objectives

2.1 Radio sounding of the neutral atmosphere

The mean radius of Venus is 6051.9 km. Venus has a retrograde rotation period of 243.025±0.001 Earth days; its orbital sidereal period is 224.7 Earth days (the solar day lasts 117 Earth days). The atmosphere consists mainly of CO_2 (~96.5%) and N_2 (~3.5%), with small amounts of other gases. Despite its slow rotation rate, the lower and middle atmosphere display a strong zonal wind structure with a period of 4–5 days ('super-rotation', i.e. in the sense of planetary rotation). Venus is shrouded by a 20 km-thick cloud layer; its surface temperature is 735K. There is no sublimation/condensation of the atmosphere as is the case for Earth and Mars (Saunders, 1997).

At low altitude (0–60 km) there appears to be an overturning of the atmosphere from equator to pole in the form of one or several meridional Hadley cells, with giant vortices at each pole recycling the air downwards. There are important questions related to the detailed structure of the low-altitude meridional atmospheric circulation and to the coupling of the polar vortices to the components of the global circulation. The driving mechanism is unknown; it may be a manifestation of vertically propagating waves, a possible carrier of momentum which then transfers its momentum via large horizontal eddy diffusion to the mean flow, which is observed in the middle atmosphere as the zonal super-rotation (Gierasch, 1975). Yamamoto & Takahashi (2003) suggest that the atmospheric angular momentum is supplied from the planetary surface. According to Izakov (2001), besides surface friction, gravity-wave drag is another method of angular momentum transport.

The middle atmosphere (60–110 km) is a transition region between the zonal super-rotation regime in the lower atmosphere and the solar-antisolar circulation in the upper atmosphere. The mechanism causing that transition is virtually unknown.

Pioneer Venus Orbiter (PVO) radio occultation data showed that the characteristics of the thermal structure in the troposphere and stratosphere regions are dependent predominantly on the latitude and only weakly on solar illumination conditions. The most striking feature is a dramatic change in the temperature structure moving from low latitudes to high latitudes. At mid-latitudes, a more distinct tropopause (~40 km altitude) begins to be evident and a growing inversion appears above the tropopause, developing as a 'collar' region between 55ºN and 75ºN (Kliore & Patel, 1982; Newman et al., 1984). However, no such collar was reported in Jenkins et al. (1994), confirming the variability of this feature.

Above an altitude of 120 km, PVO observations show relatively low dayside temperatures (300K) despite the proximity of Venus to the Sun, and a sharp collapse across the terminators to very low nightside temperatures (110K), (Keating et al., 1979). This is in great contrast to the expected thermospheric behaviour and has no counterpart anywhere in the Solar System. Global characterisation of the density and temperature structure is still needed to understand this effect.

The temperature profiles gained by radio occultation techniques also offer the possibility of studying the stability of the atmosphere by deriving the buoyancy or Brunt-Väisälä frequency (Hinson & Jenkins, 1995).

The same authors also showed that small-scale oscillations (temperature amplitudes of up to 10K) can be caused by vertically propagating gravity waves, which can be identified in retrieved temperature profiles and in scintillations in received signal intensity recorded with high time resolution. Gravity waves seem to be a persistent global feature of the Venusian atmosphere.

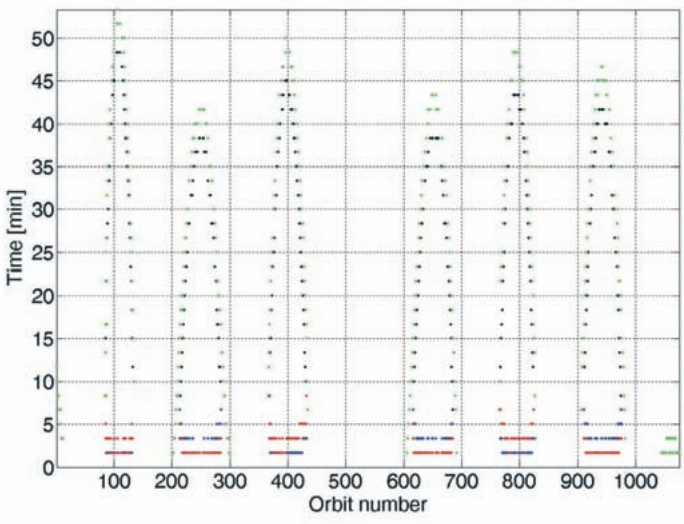

Fig. 1. Occultation seasons for VeRa for the nominal (orbit number < 500) and extended mission (orbit number > 500). Black dots indicate the duration of a pure planetary occultation, green dots show the duration of the occultation assuming an atmosphere/ionosphere with an altitude of 240 km.

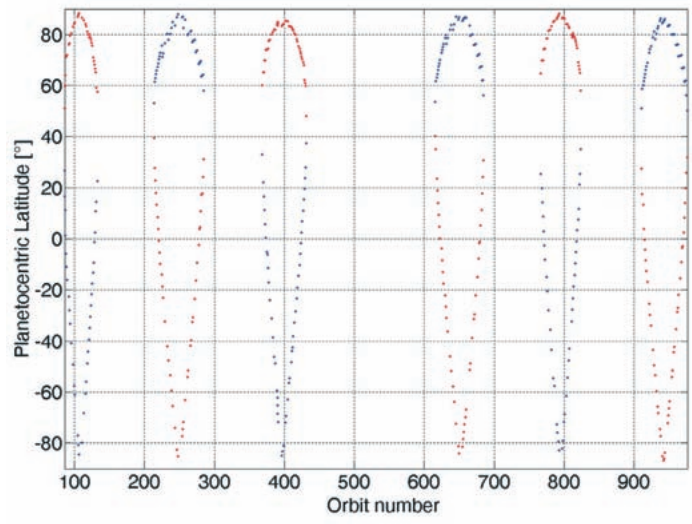

Fig. 2. Distribution of planetocentric latitudes for occultation ingress and egress (assumed to be at the planetary surface) for the nominal and extended missions. Red dots mark occultation ingress, blue dots occultation egress.

At altitudes below 40 km atmospheric and defocusing losses significantly limit the quality of the observations. Below ~32.3 km, the atmosphere is critically refractive, making it principally inaccessible to radio occultations.

Important issues concerning the atmosphere of Venus are discussed in Titov et al. (2001), Taylor (1997, 2002) and Moroz (2002).

The distribution and duration of the various VeRa occultation seasons are given in Figs. 1 and 2 (based on orbit information from Rodriguez-Canabal et al., 2003). It is important to know that an occultation pass can last up to 50 min, depending on the orbital/geometrical constellation between spacecraft, Venus and Earth. Occultations occur at all planetocentric latitudes.

2.1.1 Measurement objectives

VeRa will globally characterise the density and temperature structure of the neutral atmosphere above an altitude of ~40 km by determining the planetocentric longitudinal and latitudinal distribution; it will determine the temperature to better than 1K. Atmospheric observations are being made for every second occultation path because, in this sufficient number, they can reveal the nature of the propagation of atmospheric waves and the transfer of angular momentum in the atmosphere.

2.2 Atmospheric absorption

It has been shown that the H_2SO_4 (g) abundance can become significant below an altitude of 50 km, reaching peaks of 18–24 ppm near 39 km before dropping precipitously below 38 km (Jenkins et al., 1991; 1994). Significant variations were found with Magellan from orbit to orbit, suggesting dynamical processes between 33 km and 200 km, and revealing information about the horizontal variability of the atmosphere in the absorbing layer below the cloud deck.

To account for this effect, the attenuation of the radio signals (S/X-band) during an occultation pass was simulated by ray-tracing techniques using the Magellan reference atmosphere given in Lee (1996). Absorptivity profiles derived from Kolodner & Steffes (1998), including the contribution from all species (CO_2, H_2SO_4 (g), SO_2 (g)), were averaged and approximated by an analytical

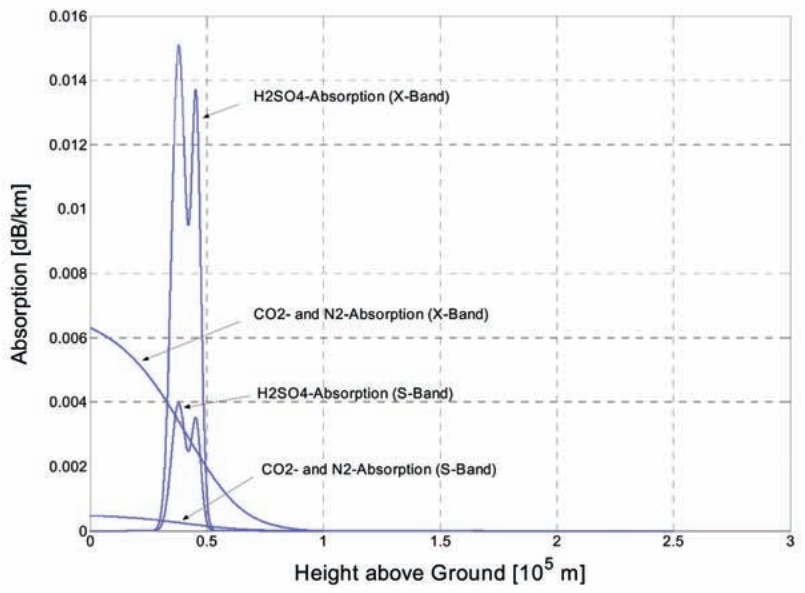

Fig. 3. Average profile of absorption *vs.* height for H_2SO_4 (g), CO_2 and N_2 in the atmosphere of Venus. Input data based on Kolodner & Steffes (1998).

function. Fig. 3 shows the result for X-band and S-band frequencies, with the expected absorption maximum at altitudes near 39 km.

2.2.1 Measurement objectives

The amplitude (power) variations of the received radio signal are recorded at a time resolution of better than 0.1 s in order to allow the determination of the abundance and spatial distribution of sulphuric acid vapour in the atmosphere, which is a tracer for atmospheric motions.

2.3 Radio sounding of the ionosphere

The absence of a planetary magnetic field at Venus leads to important differences with the structures of Earth's ionosphere. The upper atmosphere of Venus is not protected by a magnetic field from direct interaction with the solar wind, which can lead to strong atmospheric escape processes. The ionospheric pressure, consisting of thermal and magnetic components, balances the dynamic pressure of the solar wind (Luhmann, 1986; Russell & Vaisberg, 1983).

The upper boundary of the ionosphere, where the plasma density shows a deep gradient, is called the ionopause. Its average location was measured with PVO's particle instruments during solar-maximum conditions; PVO made radio occultation measurements during solar-minimum conditions (1980–1986) (Mahajan & Diwivedi, 2004). The altitude range of the ionopause during solar-minimum conditions is 200–400 km; during solar-maximum it is 400–800 km. The typical ionopause electron density is 10^8 el m^{-3}.

Owing to the orbital conditions and the rather low expected height of the ionopause, radio occultation is the only experimental technique available to Venus Express that can measure the location of the ionospheric boundary during the solar-minimum conditions of the mission. Ionospheric sounding will not be feasible when Venus is at superior solar conjunction (±10° elongation or ±40 solar radii with respect to the solar disc in the plane of sky).

The sensitivity of the VeRa experiment is of the order 100 el cm^{-3}; the altitude resolution of the derived electron density profile is around 100 m or better.

These studies will also contribute to an understanding of the development of Earth's environment during the epochs of weak magnetic field (Titov et al., 2001).

2.3.1 Measurement objectives

VeRa is investigating the ionospheric structure from ~80 km to the ionopause (< 600 km), which allows the study of the interaction of solar wind plasma with the atmosphere. VeRa, the MAG dc-magnetometer and the ASPERA plasma analyser provide complementary plasma observations in or close to the Venus ionosphere.

2.4 Bistatic radar

By measuring echoes at normal incidence, PVO found regions on the surface of Venus that exhibited unexpectedly high radar reflectivity (up to 0.4; Pettengill et al., 1982). It was later found that these regions were also associated with low surface emissivity (~0.54; Ford & Pettengill, 1983). The lowest emissivities appear in topographically high areas (3 km above the mean planetary radius for mountains; 5 km above the mean for Maxwell). This suggests that a phase-change or differences in chemical weathering occur at about 6055 km radius (Tyler et al., 1991). Elevated regions identified were Ovda Regio, Thetis Regio, Maat Mons, Ozza Mons, Theia Mons and Rhea Mons. The PVO results were confirmed and refined using Magellan data (Pettengill et al., 1992, Table 2).

Similarly, exotic phase-changes in materials at the upper levels of mountains were demonstrated by observing variations in polarisation from Maxwell Montes with a bistatic scattering experiment conducted with the Magellan orbiter (Pettengill et al., 1996). The results led to the conclusion that a thin coating of semiconductor material (elemental tellurium) could explain the observations. At very high altitudes (above 6056 km in the equatorial regions), the emissivity switches back to values that are more typical of the plains. It should be noted, however, that the prominent Maat Mons volcano differs from other Venus highlands in not exhibiting high radar reflections at its summit (Klose et al., 1992; Robinson & Wood, 1993).

Recent analyses propose alternatively that high dielectric-constant compounds of lead and bismuth condense in the Venusian highlands (Schaefer & Fegley, 2004). Also discussed is the role of magnetic minerals and ferrimagnetic phase transitions in highlands (Kreslavsky et al., 2005), as well as the role of ferroelectric material (Arvidson et al., 1994).

2.4.1 Measurement objectives

Bistatic radar measurements are, in principle, possible throughout the whole mission. In order to receive sufficiently strong radar reflection signals, the experiment is being conducted mainly in the specular reflection mode using large ground stations (70 m Deep Space Network antennas) at Venus-Earth distances of < 1.2 AU and at low altitudes of the satellite (< 15 000 km).

2.5 Gravity effects

Magellan answered many questions about the planet's geophysical and geological histories but it also raised new questions. Venus is a one-plate planet and thus does not experience Earth-like plate tectonics. The tectonic style of this planet is, however, not clearly understood. A strong link with the underlying mantle dynamics is suspected. In this context, the structure of the lithosphere is a key parameter because it plays a major role in the mantle dynamics and in the tectonics of the surface.

The best determination of the gravity field was computed from Magellan data and corresponds to a gravity field developed with spherical harmonics up to degree and order 180 (Konopliv et al., 1999). However, owing to some gaps in the tracking of the spacecraft (especially at low pericentre passes), the resolution of this model is not uniform at the surface of the planet. VeRa offers the possibility of studying the gravity field with improved resolution within the longitude and latitude intervals 140–220°E and 40–80°N. The orbital tracks are

Observation Type	*Science Objectives*	*Spacecraft Mode*	*Receiver Mode*	*Radio Links*
Occultation	Atmospheric density, temperature and pressure profiles. H_2SO_4 absorbing layer Ionospheric structure Atmospheric waves	ONED USO driven Carrier only	OL CL	X and S down
Bistatic Radar	Planetary surface dielectric properties and roughness	ONES USO driven Carrier only	OL	X and S down both polarizations
Solar Corona-Solar Wind	Solar corona structure, Solar wind acceleration region, electron density, CME	TWOD coherent	CL, OL Ranging mode	S up X and S down both polarizations
Gravity	Gravity anomalies	TWOD coherent Carrier only	CL	X up X and S down

Table 1. Observation types, scientific objectives, radio-frequency transmission modes and ground station configurations for VeRa.

separated by about 1.5º at altitudes close to pericentre, corresponding to ~80 km along a parallel at perigee. At pericentre, the speed is near 9 km/s so a sampling of 10 s ensures a sampling of 90 km in latitude.

A preliminary analysis shows that gravity campaigns are possible in the time periods: 26 August – 1 November 2006; 23 June – 2 July 2007; 26 December 2007 – 1 March 2008.

2.5.1 Measurement objectives

As the longitudes cover a range of about 80º, the mapping can be achieved in about 60 successive orbits of Venus Express. The 'TWOD' transmission mode (Table 1) will be used by the spacecraft. The orbits selected need to be occultation-free around pericentre and to be outside of solar conjunction periods. The sampling rate will be 10 s. The main area covered is Atalanta Planitia, is a low-altitude basin with a diameter of ~1500 km and a depth of ~2 km. The resolution of the Magellan gravity field model is estimated to be at a wavelength as low as ~475 km (Konopliv et al., 1999). Given the Venus Express pericentre altitude of about 250 km and the optimal data sampling rate that can be reached, an improvement of this wavelength resolution to about 100–150 km is expected. In turn, the understanding of the lithosphere structure under this area might be improved on the basis of the analysis of the topography-gravity relationship (Leftwich et al., 1999).

2.6 Solar corona and solar wind

Venus will move into superior and inferior conjunctions with the Sun several times during the mission. The view of the planet's path in the plane of the sky around the time of conjunctions is shown in Fig. 4. During superior conjunctions, which cannot be used for high-quality data transmission from the spacecraft, corona and solar wind effects can be studied. During superior conjunctions, measurements in the TWOD mode will be performed for several hours each day when Venus is within 10º of the Sun or 40 radii from the solar disc as seen from Earth in the plane of sky.

The inferior-conjunction measurements will be carried out for several hours

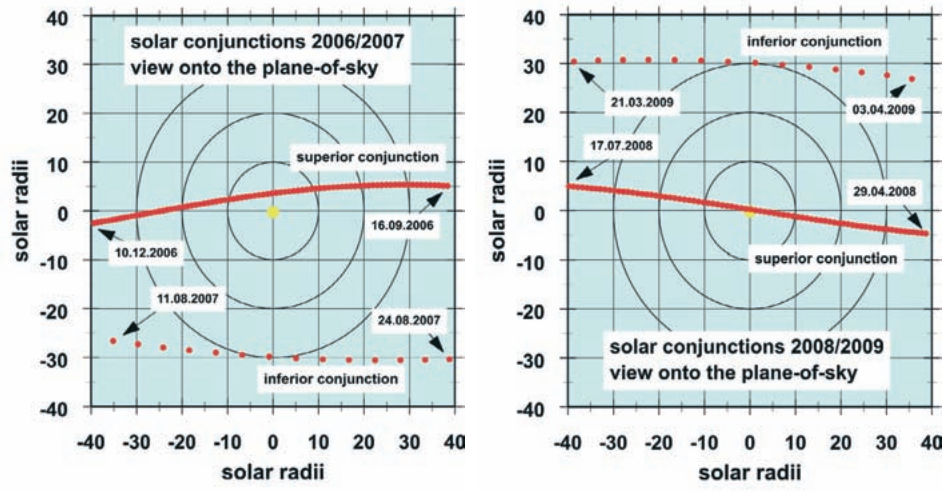

Fig. 4. First (left) and second solar conjunction pair.

when Venus is at 10º elongation (40 solar radii), and 5º elongation (20 solar radii) on both sides of the solar disc, and also near the point of conjunction.

2.6.1 Measurement objectives

It is proposed to derive electron density profiles in the structured corona, solar wind speed, turbulence spectra in the source regions of fast and slow solar wind streams from coronal holes and streamers, respectively, and to detect, identify and describe the spatial and temporal evolution of the shockfronts of coronal mass ejections (Bird et al., 1994; Pätzold et al., 1995, 1996; Karl et al., 1997). At inferior conjunction, the lowest level of solar wind turbulence will be measured and recorded for calibration purposes.

3. Measurement Technique

3.1 The spacecraft radio subsystem and its transmission modes

The possible radio-frequency transmission modes are shown in Fig. 5. The prime ground station for the VeRa measurements is New Norcia (NNO) in Australia. NASA Deep Space Network (DSN) support for specific mission phases is available. The observation modes, transmission modes and ground station configurations for Venus Express are listed in Table 1. Fig. 6 presents a block diagram of the onboard radio subsystem. The 1.30 m-diameter main high-gain antenna (HGA1) with two feeds (X- & S-band) is used for VeRa. The transponder X-band signals are amplified by two redundant 65 W travelling wave tube amplifiers (TWTAs), while the S-band signal is transmitted by a 5 W amplifier. The gain of the HGA1 antenna is 37 dBi (X-band) and 25.7 dBi (S-band) (Astrium, 2004).

3.2 Ray propagation in media

The atmosphere/ionosphere may be sounded before or after an occultation, when, as seen from Earth, the spacecraft disappears behind the planet (ingress) or it emerges from behind (egress). There is a range of occultation conditions, from grazing to diametric. The signal ray path bends owing to the neutral and ionised regions of the atmosphere (Fig. 7). Physical parameters such as bending angle and refractivity can only be derived after the observed radio frequency has been corrected for the Doppler effect caused by the relative motion of the spacecraft and ground station against the effects that would exist without the influence of an atmosphere. Theses effects ('predicts') are determined by the Radio Science Simulator software package (RSS; Selle et al., 2004).

Assume that a satellite with radial velocity v transmits a carrier signal with the

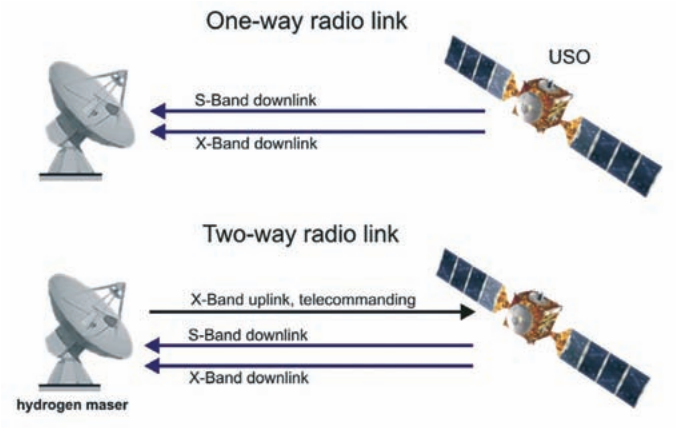

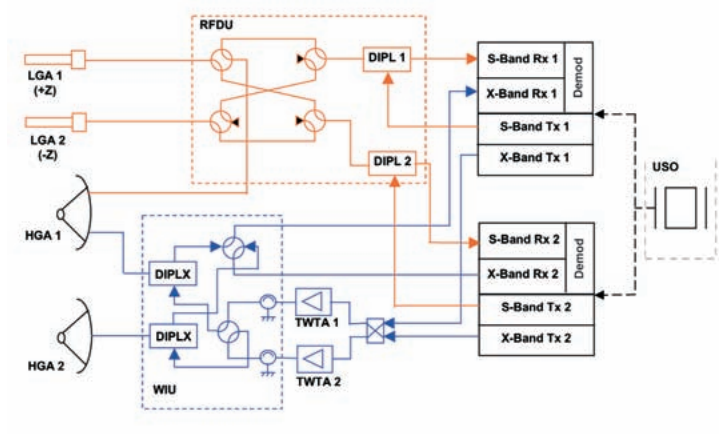

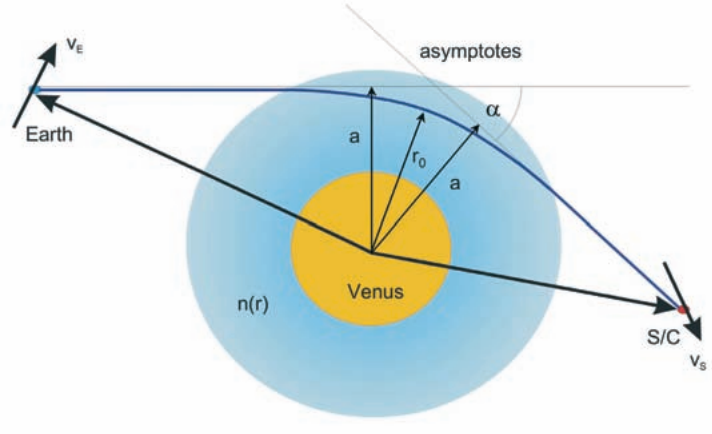

Fig. 5 (top left). Transponder configuration and transmission modes of Venus Express. The ultrastable oscillator (USO) serves as the onboard reference frequency source in the one-way transmission mode. ONED: uncoherent one-way dual-frequency downlink transmission; TWOD: coherent two-way dual-frequency downlink transmission.

Fig. 6 (top right). The Venus Express redundant radio subsystem. (Astrium, 2003)

Fig. 7 (left). Geometry used for calculation of an electromagnetic wave refraction in the atmosphere of Venus during an occultation. Ray path closest approach distance r_0 and α are related to the impact parameter *a* (asymptote closest approach distance) and index of refraction *n*(r).

frequency f_T and that the ground station receives the signal at a frequency f_E shifted by Δf with respect to f_T (one-way mode). When the wave was propagating through an ionised medium (plasma) with the local plasma density N_e (m^{-3}), we then obtain for the observable Δf in the non-relativistic case (with ds being the incremental length element along the propagation path, and c is the speed of light):

$$\Delta f\,(Hz) = f_T - f_E = f_T \frac{v}{c} - \frac{40.3}{c\,f_T}\frac{d}{dt}\int_T^E N_e\,ds \qquad (1)$$

The frequency shift of the carrier frequency is composed of two parts – the classical Doppler shift due to the orbital motion of the satellite and the dispersive effect of the varying total integrated electron density content TEC (m^{-2}; unit = 1 Hexem = 10^{16} el m^{-2}) along the path of propagation. Gravitational and atmospheric effects are contained in the first part and can be separated from the dispersive part by employing the dual-frequency technique whereby two signals are transmitted simultaneously from the spacecraft in the ONED mode using the USO as the onboard coherent reference frequency (Häusler et al., 2003).

The differential Doppler frequency δf from two different frequencies but related by a constant 11/3 ratio for one-way propagation leads to:

$$\delta f = \Delta f_s - \frac{3}{11}\Delta f_x = \frac{-40.3\left[\frac{m^3}{s^2}\right]}{c}\, f_S\left(\frac{1}{f_S{}^2} - \frac{1}{f_X{}^2}\right)\frac{d}{dt}\int N_e\,dl \qquad (2)$$

where s and x refer to S- and X-band, respectively. This relationship allows conclusions to be drawn about the time-derivative of the TEC:

$$\frac{d}{dt}TEC = \frac{d}{dt}\int_T^E N_e\, dl \tag{3}$$

and the index of refraction n for an ionised medium. The index of refraction n (< 1) is related to the medium's electron number density N_e (m^{-3}) and the signal's frequency to second order in $1/f$:

$$n = 1 - \frac{40.3\left[\frac{m^3}{s^2}\right] N_e}{f^2} \tag{4}$$

The results of a ray-tracing Doppler simulation (one-way mode) for the occultation pass on orbit 105 using the Magellan reference atmosphere (Lee, 1996) and a model ionosphere are shown in Fig. 8. In the neutral atmosphere, the S-band Doppler residuals are a factor 4 smaller than those for the X-band signals. The scaling of the Doppler profile shown does not allow any of the ionospheric structure to be resolved.

A second important observable is the classical group delay, τ, of an electromagnetic wave, given by:

$$\tau(s) = \int_T^E \frac{ds}{v_{gr}} = \frac{s}{c} + \frac{40.3}{c f^2}\int_T^E N_e\, ds \tag{5}$$

The first part of the above equation represents the vacuum light travel time (group delay), while the second part represents the dispersive group delay and allows us to determine the TEC along the propagation path in a similar way to the Doppler effect. Using the two-way mode, the above formulae have to be adopted accordingly.

By using the differential dual-frequency method, the non-dispersive effects can be eliminated. This allows us to extract the TEC directly:

$$\delta\tau = \tau_s - \tau_x = \frac{40.3\left[\frac{m^3}{s^2}\right]}{c}\left(\frac{1}{f_s^2} - \frac{1}{f_x}\right)TEC \tag{6}$$

where $\delta\tau$ is the differential group time delay.

3.3 Relativistic corrections

The measured Doppler frequency shift contains relativistic contributions. Assuming a system T (satellite, transmitter) is transmitting the frequency f_T, and a system E (Earth ground station) receives the frequency f_E, the shift in frequency can be determined to second order in v/c by (Soffel, 1989; Krisher, 1993; Schneider, 1996; Häusler et al. 2003):

$$\frac{f_E}{f_T} \approx \frac{1 - \hat{\mathbf{n}}\cdot\boldsymbol{\beta}_E + \frac{1}{2}\beta_E^2 - \phi_E/c^2}{1 - \hat{\mathbf{n}}\cdot\boldsymbol{\beta}_S + \frac{1}{2}\beta_S^2 - \phi_S/c^2} \tag{7}$$

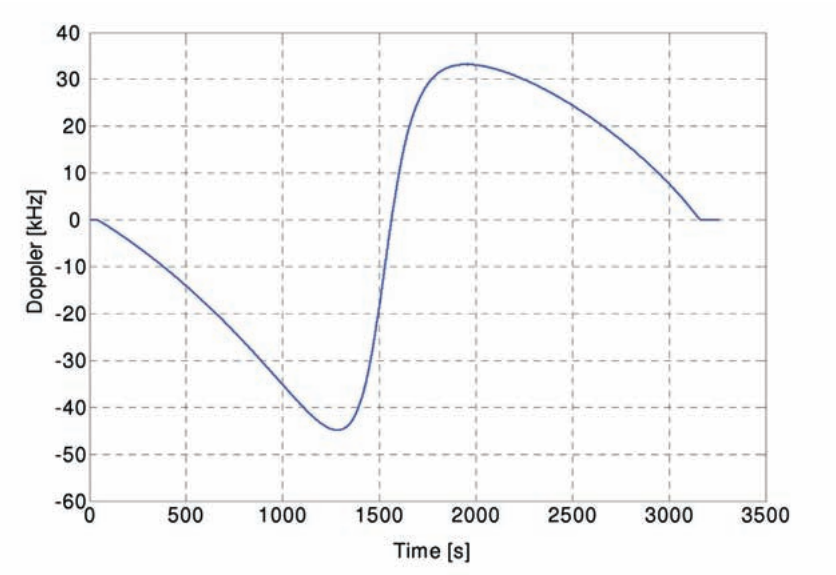

Fig. 8. Atmospheric/ionospheric media contributions to the Doppler frequency shift during the occultation pass on orbit 105 (Remus, 2004).

We define $\boldsymbol{\beta} = \mathbf{v}/c$, with $\hat{\mathbf{n}}$ being a unit vector pointing from T to E, i.e. in the direction of the signal propagation at the time the signal is radiated, including the general relativistic time delay. $\mathbf{v}_T$ is the coordinate velocity of T, and $\mathbf{v}_E$ the coordinate velocity of the ground station at the time of signal emission and reception. Barycentric coordinates are used. All relative velocities must be Lorentz-transformed. ϕ_E and ϕ_T are the gravitational potentials of E and T. The potential of the ground station contains the centrifugal potential of the Earth. The contribution of the gravitational potential (gravitational redshift) is significant. It reaches ~100 Hz at X-band in the one-way mode.

The group delay (ranging signal) must also be corrected for the effect of General Relativity (Shapiro, 1964; Reasenberg et al., 1979). Near superior conjunction, the additional range delay (two-way) can amount to ~0.2 ms, being equivalent to an error in distance by 30 km or an apparent TEC value of ~4 x 10^5 / 4 x 10^4 Hexems at S/X-band, respectively. Further details are given in Häusler (2002) and Häusler et al. (2003).

3.4 Light-time correction

When deriving the planetary velocity vectors from the ephemeris data, the effect of the finite speed of light (light travel time) must be included in order to predict the Doppler and range values. For a planetary mission like Venus Express, the light travel time can amount to 14 min. Special routines using an iterative procedure were developed for the RSS.

3.5 Earth's tropospheric and ionospheric corrections

The neutral atmosphere is a non-dispersive medium with respect to radio waves up to frequencies of 15 GHz. The refractive index n, however, is dependent on air pressure, temperature, humidity and zenith angle. The effect is a path delay that reaches 2.0–2.5 m in the zenith direction and increases approximately with the cosecant of the elevation angle, yielding about a 20–28 m delay at a 5° elevation angle, independent of the frequency. The tropospheric contribution varies slowly with time compared to the actual observation time during occultation at Venus and leads therefore to a measurable but mainly constant additional Doppler bias of the order of 1.5 mm/s during a full day of ground station tracking. Further details on modelling techniques are discussed in Häusler et al. (2003).

The ionospheric refraction leads to a reduction of group velocity and an

increase in phase velocity. The refractive index depends on local time and geomagnetic activity. The delay reaches typically 0.1–2 ns (3–60 cm) in the zenith direction at 8.4 GHz.

Further details of the modelling techniques are discussed in Sovers et al. (1998) and Häusler et al. (2003).

3.6 Reference systems and time basis

The planetary ephemeris data are determined in the RSS by the JPL/DE405 program using J2000 as the inertial reference frame. The time basis selected for the independent variable 'time' is the Barycentric Dynamical Time (TDB or T_{eph}). It is therefore necessary to match TDB (T_{eph}) time with UTC time in the prediction software routine.

The spacecraft onboard time (OBT), which synchronises the precise execution of the onboard commands, must be controlled by ground command. This includes leap-second and DUT1 (=UT1–UTC) forecasts generated by the International Earth Rotation and Reference Systems Service (IERS), as well as light-time corrections. These contributions are contained in the prediction and simulation software of VeRa.

In addition, the fact that the Earth-fixed reference system, the International Terrestrial Reference System (ITRS), is not inertially fixed in space also has to be considered. The coordinates of a vector describing the position of a ground station in the geocentric ITRS frame must therefore be transformed according to the motion of the Earth's equatorial and orbital plane and its rotation axis into an inertially fixed reference system. This is the International Celestial Reference System (ICRS), its fundamental plane being closely aligned with the mean equator at J2000. The transformation involves precise consideration of planetary and lunisolar precession, Earth's rotation, nutation and polar-motion effects. Further details are given in Häusler et al. (2003).

4. Derivation of Atmospheric Parameters

4.1 The measured Doppler frequency shift and its contributions

The dense atmosphere of Venus causes ray bending of the microwave carrier signal along its path, accompanied by a change of the phase of the wave (Fig. 7). Owing to the orbital motion of the satellite, this variation is time-dependent and is reflected as a Doppler frequency shift at the ground station. The total Doppler frequency shift Δf measured during an occultation can be expressed by:

$$\Delta f = \Delta f_0 + \Delta F \tag{8}$$

The 'residuum' ΔF is the contribution to the Doppler effect caused by the medium alone, and Δf_0 is the vacuum contribution to the Doppler effect (depending on the satellite velocity vector projection onto the satellite-ground station line of sight). Hence, the ΔF is determined by the difference between the measured Doppler effect Δf and the predicted vacuum effect Δf_0. In consequence, any error in the Doppler predictions leads to errors in the derived medium effects. Frequency measurements on the ground can be made with an accuracy of 1 mHz, equivalent to a relative frequency error of 10^{-13}. All theoretical models (planetary ephemeris data and orbital information) and the subsequent numerical calculations must be oriented towards this accuracy requirement.

4.2 The Abel inversion

Using the general principles of optics (Born & Wolf, 1970), it can be shown that, for a radially symmetric atmosphere, the asymptotic bending angle α is related to the refractive index n by:

$$\alpha(a) = -2a \int_{r=r_o}^{r=\infty} \frac{1}{n} \frac{\partial n}{\partial r} \frac{dr}{\sqrt{(nr)^2 - a^2}} \tag{9}$$

α being the ray impact parameter (Fig. 8) and r_0 is given by Bouguer's Rule:

$$r_o = \frac{a}{n(r_o)} \tag{10}$$

which means that a ray with impact parameter α will penetrate a spherically symmetric atmosphere until it reaches a radius r_0.

In a well-mixed atmosphere, the density gradient is linked to the gradient of the refraction index by a simple relation:

$$\frac{\partial n}{\partial r} = K \frac{\partial N_t}{\partial r} \tag{11}$$

K depends on the chemical composition of the atmosphere, and N_t is the number density of the atmosphere.

The variation of the bending angle α, the ray asymptote and the refractive index are linked through an Abel transformation (Fjeldbo et al.,1971):

$$\ln n(r_{o1}) = -\frac{1}{\pi} \int_{a=a_1}^{a=\infty} \ln\left\{ \frac{a}{a_1} + \left[\left(\frac{a}{a_1} \right)^2 - 1 \right]^{1/2} \right\} \frac{d\alpha}{da} da \tag{12}$$

which is equivalent to

$$\pi \ln n(r_{01}) = -\int_{a=a_1}^{a=\infty} \frac{\alpha(a)}{\sqrt{a^2 - a_1^2}} da \tag{13}$$

a_1 is the asymptotic impact parameter for a ray with radius of closest approach r_{01}. For spherical atmospheres, if $\alpha(a)$ is known, the corresponding refractivity profile can be found exactly (neglecting multipath conditions). The asymptotic bending angle $\alpha(a)$ is a function of the residual Doppler frequency (which is the difference between the measured and predicted Doppler frequency) and precisely reconstructed quantities such as the velocity and position vectors of the transmitter and receiver system (Yakovlev, 2002). Eq. 13 allows the refractive index at $r = r_{01}$ to be determined as a function of planetocentric latitude and longitude.

4.3 Atmospheric parameters

The relation between the refractive index n and the refractivity μ is:

$$\mu = (n–1) \times 10^6 \tag{14}$$

To compute pressure and temperature from refractivity, it is necessary to know the atmospheric composition. Since the bulk of the neutral atmosphere of Venus is composed of non-polar gases (96.5% CO_2 and 3.5% N_2) and is well mixed, the number density N_t (m^{-3}) is related to the refractivity μ by a simple equation (adopted from Jenkins et al., 1994)

$$N_t = K \mu \qquad \text{with K} = 8.21 \times 10^{22}\ m^{-3} \tag{15}$$

The presence of trace gases or small uncertainties in composition does not introduce large errors in the profiles. For high-precision analyses, however, the

composition must be known or treated as a variable. The total refractivity μ is independent of frequency at microwavelengths and inversely proportional to frequency squared in the ionosphere:

$$\mu(r) = \frac{p(r)}{\kappa\ kT(r)} - 40.3\left[\frac{m^3}{s^2}\right]\frac{N_e(r)}{f^2}\ 10^6 \tag{16}$$

The ideal gas law relates pressure, temperature and number density of the gas. Since hydrostatic equilibrium applies very accurately throughout well-mixed atmospheres, we can derive from the refractivity profiles and known atmospheric constituents the vertical structure of the neutral atmosphere by integrating the equation of hydrostatic equilibrium and applying the ideal gas law (Eshleman, 1973; Jenkins et al., 1994; Yakovlev, 2002):

$$\begin{aligned} N_t(r) &= \kappa\ \mu(r) \\ p(r) &= p_{top} + \overline{m}\int_r^{r_{top}} N_t(r)\, g(r)\, dr \\ p_{top} &= \mu_{top}\ \kappa\ kT_{top} \\ T(r) &= \frac{\mu_{top}}{\mu(r)} T_{top} + \frac{\overline{m}}{k\ N_t(r)} \int_r^{r_{top}} N_t(r) g(r) dr \end{aligned} \tag{17}$$

where $p(r)$ is the atmospheric pressure, $g(r)$ is the acceleration due to gravity, k is Boltzmann's constant, $\overline{m}$ is the mean molecular mass, $N_t(r)$ is the total number density, r is distance along the local vertical, and r_{top} is an adopted 'top' of the atmosphere. T_{top} is the required boundary condition at the top of the neutral atmosphere. The integration of the profile is not very sensitive to this value for the lower atmosphere. The associated flow diagram is shown in Fig. 9.

The first step in estimating the accuracy of the parameter determination is an analysis of the radio link budgets and the carrier-to-noise power ratio in a VeRa experiment (see Section 5.6). A thorough mathematical treatment of the error estimation is presented in Lipa & Tyler (1979).

4.4 Atmospheric defocusing loss

Atmospheric defocusing has to be taken into account when predicting and interpreting the received signal strength data. It is caused by the gradient in refractivity with respect to radius, which distorts the shape of the beam by spreading it in the plane of the occultation and compressing it in the orthogonal direction. The refractive defocusing τ (dB) does not depend on frequency and is estimated from the ray-path parameters and the occultation geometry (Eshleman, 1973):

$$\tau = 10\log\left(\cos\alpha - D\frac{d\alpha}{da}\right)\ \text{(dB)} \tag{18}$$

where D is the distance from spacecraft to the crossing of the asymptotes (Fig. 7).

Using the Magellan model atmosphere (Lee, 1996) and a typical Venus Express orbit, the defocusing loss in an occultation pass was determined with a ray-tracing program (Fig. 10). It can be seen that the defocusing loss depends strongly on the radial distance from the spacecraft to the planet.

4.5 Spatial resolution of atmospheric measurements

The size of the first Fresnel zone is a convenient measure of the altitude resolution

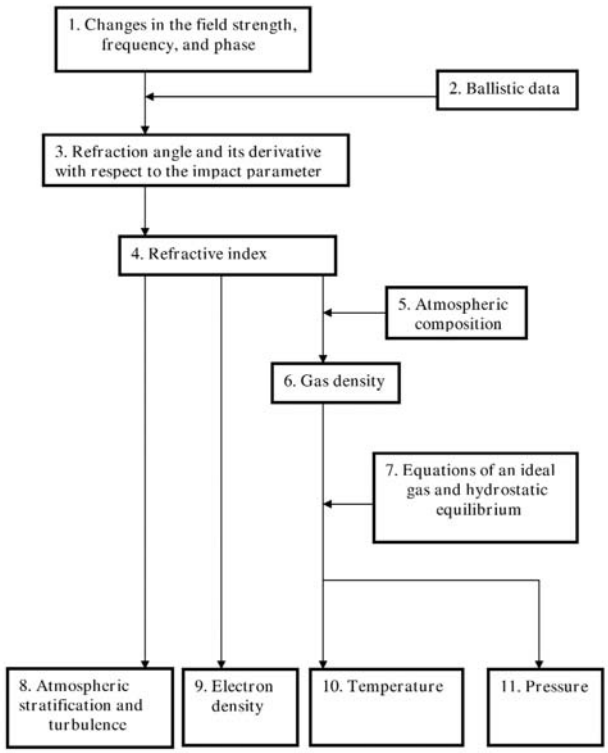

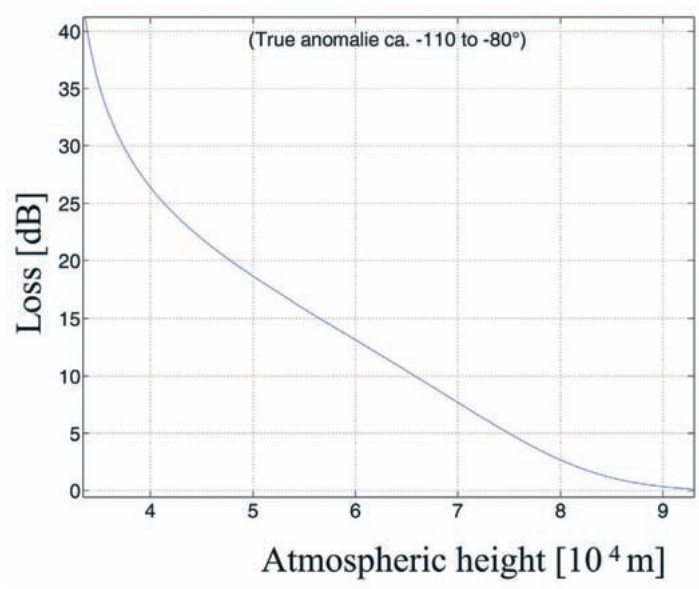

Fig. 9 (left). The principle of evaluating atmospheric and ionospheric parameters by the radio occultation technique (Yakovlev, 2002).

Fig. 10 (above). Defocusing loss for a typical occultation (Häusler et al., 2004a)

that can be achieved by the occultation experiment. Refraction has the effect of compressing these zones in the vertical dimension, from circular to elliptic. The result is an improved altitude resolution in regions that cause defocusing; conversely, the resolution is reduced in those portions that produce focusing (Fjeldbo & Eshleman, 1969).

With D the distance from the transmitter to the atmospheric reference point and assuming that D is considerably smaller than the distance d from the planet to the receiver, we obtain with wavelength λ for the horizontal diameter r_{fz} of the Fresnel zone (horizontal resolution):

$$r_{fz} \sim \sqrt{\lambda D} \tag{19}$$

an expression independent of d amounting to $r_{fz} \sim 600$ m at X-band for a typical $D = 10\,000$ km. For the vertical resolution we obtain:

$$r_{refrac} = r_{fz} \times \sqrt{\frac{I_{refrac}}{I_o}} \tag{20}$$

where the square root expression stands for the defocusing loss caused by refraction. With the defocusing loss shown in Fig. 10, we obtain for the vertical resolution at medium-low altitudes values that can be considerably smaller than the Fresnel zone. Special techniques such as back-propagation have therefore been developed by the Stanford group to recover the complete profile to resolve diffracting structures to vertical solutions an order of magnitude better than the Fresnel scale (Han & Tyler, 2003). It also provides a means of deciphering multipath propagation (Karayel & Hinson, 1997; Hinson et al., 1998).

It may be possible to resolve spatial structures and to separate longitudinal from latitudinal effects by using signal detection with several ground stations. For VeRa, a spatial resolution at the Venus surface of $\Delta x \sim 1$ km can be

Table 2. Radio-frequency system parameters for the Venus Express spacecraft and ground stations.

Ground station	*DSS 63 (or equivalent)*	*NNO*
Diameter (m)	70	35
Gain (dB) S-Band rx	63.3	55.8
Gain (dB) X-Band rx	74.3	68.2
System Noise Temp. (K)		
S-Band	20	47.9
X-Band	25	74
G/T(dB/K)		
S-Band	50.3	39
X-Band	60.3	49.5
Venus Express Spacecraft		
EIRP (dBW)		
S-Band	32.7	
X-Band	55.1	

expected. The Very Long Baseline Interferometry (VLBI) phase-referencing technique was successfully demonstrated for the Vega and Giotto missions (Sagdeev et al., 1992; JIVE, 2003). Further, information about the vertical structure of zonal winds in the atmosphere was obtained in the Pioneer Venus project using differential long-baseline interferometry (Counselman et al., 1980).

4.6 Link budgets

For the first occultation season in the Venus Express mission the mean distance of Earth to Venus is ~1.5 AU; for the second occultation season it is 1.65 AU, followed by 0.8 AU for the third. Table 2 summarises the radio-frequency parameters of the spacecraft and selected ground stations. Table 3 presents the link budgets, including system, absorption and defocusing losses. From a link budget point of view, the third occultation season is by far the most favourable: it has an improvement of 6.3 dB over the second season. The ground stations used for VeRa are ESA's New Norcia and a NASA DSN station equivalent to DSS-63 to cover situations of low signal-to-noise power ratios.

4.7 Doppler signal open-loop recording

The physical quantities measured during an occultation pass are the Doppler frequency shift and the amplitude of the received radio signal at two frequencies. The dual-frequency mode (ONED) is used to separate the plasma contribution from the neutral atmosphere contribution, and the right-hand circular (RHC) polarised signals are recorded in open-loop at the ground station. The Doppler shift can be dynamically compensated by the ground station by special local oscillator (LO) tuning (3rd-order polynomial fit). The incoming signals are sampled in both frequencies and RHC polarisation by the intermediate frequency modem system (IFMS) in New Norcia or the corresponding DSN ground station with a sample rate of up to 100 000/s (both I and Q channels) to cover the expected frequency deviations of the carrier signal. For illustration, the expected Doppler profile as measured during the occultation phase of sample orbit 105 is shown in Fig. 11. The corresponding Doppler signal from orbital effects alone is shown in Fig. 12. (The effect of the media alone was shown in Fig. 8.)

The variance of the Doppler frequency shift owing to thermal noise contributions in a radio link can be calculated as (Yuen, 1983):

	S-Band 2.3 GHz		X-Band 8.4 GHz	
Distance (AU)	0.28	1.72	0.28	1.72
Overall C/N_0 (dBHz) NNO/DSS 63 (w/o losses)	45.1/56.4	29.3/40.3	66.8/77.6	51.0/61.8
Losses (dB) for various minimum probed altitudes r_0				
Defocusing				
40 km	26.4	26.4	26.4	26.4
42 km	24.0	24.0	24.0	24.0
50 km	18.0	18.0	18.0	18.0
Absorption				
40 km	2.1	2.1	14.7	14.7
42 km	1.8	1.8	10	10
50 km	0.1	0.1	0.5	0.5
Overall C/N_0 (dBHz) NNO/DSS 63 (including losses)				
40 km	16.6/27.9	0.8/12.1	25.7/36.5	9.9/20.7
42 km	19.3/30.4	3.5/14.8	32.8/43.6	17/27.8
50 km	27/38.3	11.2/22.2	48.3/59.1	32.5/43.3

Table 3. VeRa signal-to-noise parameters for two ground stations (NNO/DSS-63) as a function of minimum probed altitude for two Venus-Earth distances, including losses (ONED transmission mode).

Fig. 11 (below, left). Predicted X-band Doppler profile (one-way mode) as measured at the ground station during the occultation on orbit 105 (Remus, 2004).

Fig. 12 (below, right). Predicted X-band Doppler profile (one-way mode, straight line) during the occultation on orbit 105 caused by orbital effects only, excluding media effects (Remus, 2004).

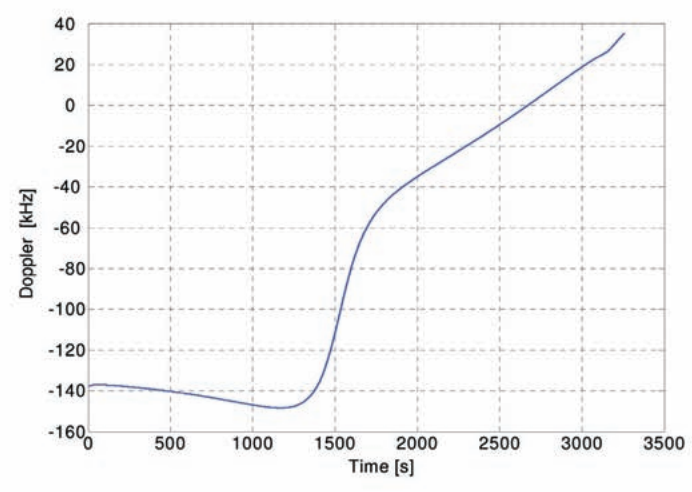

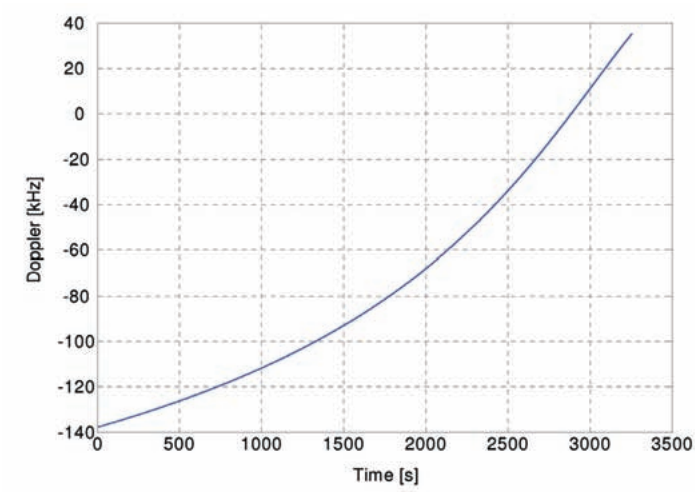

$$\sigma_f = \frac{\sqrt{2BN_o/C}}{2\pi T} = \frac{\sqrt{N/C}}{2\pi T} \quad \text{(Hz)} \qquad (21)$$

where $2B$ is the noise bandwidth to be considered, C is the carrier power, and T is the integration time.. The resulting velocity error is:

$$\sigma_v = \frac{c\sqrt{2BN_o/C}}{4\pi f T} \quad \text{(m/s)} \qquad (22)$$

In the following, the calculations are based on a noise bandwidth $2B$ of 1 Hz and an integration time of 1 s. At minimum ray-path altitudes below ~60 km, it is possible to integrate the signals at the expense of time resolution for the benefit of C/N and frequency resolution improvement. Integration times of 1–100 s appear to be practical. Such integration times can be justified because time variations involving the complete atmosphere are expected to occur at much longer time scales and can be detected only from one orbit to the next.

The variance of the Doppler frequency shift owing to oscillator phase noise and transponder internal noise contributions can be derived from the Allan variance $\sigma_y(\tau)$ (see Section 6.2 and Hagl et al., 2004; Häusler et al., 2004b; Häusler & Remus, 2004; Mattei et al., 2004). Integration times τ are assumed to be 1–100 s after a warm-up time of 30 days: $\sigma_y(\tau) \leq 3 \times 10^{-13}$.

In the Rosetta mission, the USO signal showed a stability after launch of less than 10^{-13} at X-band (Pätzold, 2004).

The frequency error σ_{AV} is related to the Allan deviation σ_y and the received frequency f by the relation:

$$\sigma_{AV} = f\,\sigma_y \tag{23}$$

Table 4 shows the Doppler frequency errors derived by Eqs. 21 and 23. The total noise contribution σ_{tot} for the one-way transmission mode is then given by:

$$\sigma_{tot} = \sqrt{\sigma_f^2 + \sigma_{AV}^2} \tag{24}$$

The analysis shows that, because of the rather low S-band transmitter power (5 W S-band *vs.* 65 W X-band), the X-band link provides better Doppler noise performance in all situations. The excellent frequency stability and phase noise performance of the USO-transponder system optimises VeRa performance, especially for the X-band link and improve the sounding of the neutral atmosphere. For large Earth-Venus distances, the sounding of the deep atmosphere can be considerably improved with a more powerful ground station than NNO, such as DSS-63 and DSS-43.

5. Gravity Anomalies

The velocity perturbation Δv_p^l of a spacecraft, coming from a given harmonic degree l of the gravitational potential of a planet of radius R and gravitational constant μ, at periapsis radius r_p, for an orbit of semi-major axis a and eccentricity e is given as (Borderies, 1991):

$$\Delta v_p^l = \sqrt{\frac{\mu}{a(1-e^2)}} \left(\frac{R}{r_p}\right)^l \sqrt{\sum_{m=0}^{l} (\bar{C}_{lm}^2 + \bar{S}_{lm}^2)} \tag{25}$$

where $\bar{C}_{lm}$ and $\bar{S}_{lm}$ are the normalised gravity coefficients.

This expected signal has to be compared with the Doppler noise expected from the radio-frequency measurements. When concentrating on Atalanta Planitia (Section 2.5), the critical harmonic degree that should be covered by VeRa is 60. With Kaula's rule and Venus gravity parameters given by Konopliv et al. (1999), the following velocity signals are obtained for the stated perigee altitudes: 0.017 mm/s at 250 km; 0.011 mm/s at 300 km; 0.007 mm/s at 350 km; 0.004 mm/s at 400 km.

From the two-way link analysis for coherent X-band transmission (Pätzold & Häusler, 2004), an Earth-Venus distance of 1.7 AU, NNO as ground station, a tracking loop bandwidth of 1 Hz and an integration time of 10 s can be expected to yield a thermal contribution to the Doppler velocity error of ~0.004 mm/s, which should make observations of gravity anomalies of the required accuracy

Ground Station NNO/DSS 63	S-Band 2.3 GHz		X-Band 8.4 GHz	
Distance (AU)	0.28	1.72	0.28	1.72
Minimum altitudes probed > 60 km		*No losses*		
Overall C/N_0 (w/o losses)	45.1/56.4	29.3/40.3	66.8/77.6	51.0/61.8
σ_f (mHz)	0.88/0.25	5.4/1.5	0.07/0.02	0.45/0.13
σ_{AV} (mHz)	0.7	0.7	2.5	2.5
σ_{tot} (mHz)	1.1/0.7	5.4/1.6	2.5/2.5	2.5/2.5
Minimum altitude probed 60 km		*With losses*		
C/N_0 (dB)	35.1/46.4	19.3/30.3	56.8/67.6	41.0/51.8
σ_f (mHz)	2.8/0.8	17/4.9	0.2/0.07	1.4/0.4
σ_{AV} (mHz)	0.7	0.7	2.5	2.5
σ_{tot} (mHz)	2.9/1.1	17.0/4.9	2.5/2.5	2.9/2.5
Minimum altitude probed 50 km		*With losses*		
C/N_0 (dB)	27/38.3	11.2/22.2	48.3/59.1	32.5/43.3
σ_f (mHz)	7.1/1.9	43/12	0.6/0.18	3.8/1.1
σ_{AV} (mHz)	0.7	0.7	2.5	2.5
σ_{tot} (mHz)	7.1/2.0	43/12.0	2.6/2.5	4.5/2.7
Minimum altitude probed 40 km		*With losses*		
C/N_0 (dB)	10.4/21.7	-5.4/5.9	19.3/30.1	3.5/14.4
σ_f (mHz)	8.3/2.3	51/14	3.0/0.9	18/5.3
σ_{AV} (mHz)	0.7	0.7	2.5	2.5
σ_{tot} (mHz)	8.3/2.4	51.0/14.0	3.9/2.7	18.2/5.9

Table 4. Expected Doppler noise at various minimum ray-path altitudes r_0 for two ground stations (NNO/DSS-63) and two downlink frequencies at two extreme Earth-Venus distances. Integration time interval = 1 s. Atmospheric absorption and defocusing losses are included.

possible for low (< 400 km) pericentre altitudes. Smaller Earth-Venus distances and/or the use of a larger ground station such as DSS-63 and a smaller tracking loop filter bandwidth can improve the quality of the results considerably.

6. Planetary Surface Properties (Bistatic Radar Experiments

There are at least three geometries for bistatic experiments: quasi-specular (discussed below), spotlight (used unsuccessfully with Magellan), and inertial (possibly useful for detecting enhanced backscatter). Quasi-specular experiments are preferred for Venus Express. The geometry is shown in Fig. 13, with the transmitter aboard the spacecraft and the receiver on the ground.

By aiming the HGA towards the specular point on Venus, the reflected power can be measured as the spacecraft moves in its orbit. (The attitude predictions for a bistatic radar experiment have to include the refraction effects of the atmosphere). Estimates of the dielectric constant can be derived from the power received in two orthogonal polarisations and comparison with Fresnel reflection coefficients. From the dielectric constant and suitable modelling, it is possible to estimate the density of the surface material. For surfaces that scatter narrowly, it should also be possible to derive estimates of cm-scale roughness.

Positions of the receiver and transmitter are given by vectors **r** and **t**. Angles of incidence and scattering at the reflection point **s** are ϕ_i and ϕ_s, respectively. In general, there is an azimuthal angle between the plane of incidence and the plane of scattering. For quasi-specular experiments the two planes are the same.

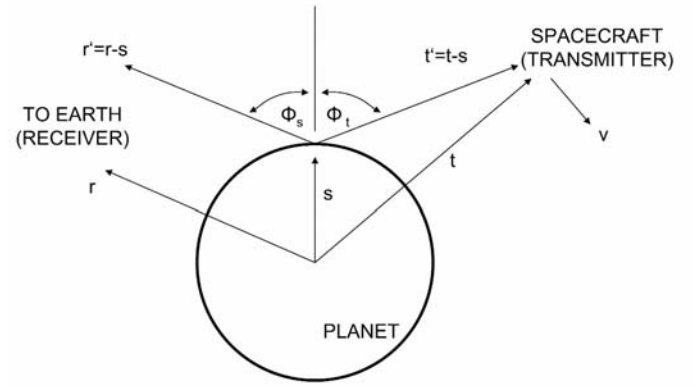

Fig. 13. Geometry for bistatic radar experiments (Simpson, 1993).

6.1 Quasi-specular experiments

For incoherent processes, the total received signal power P_R is given to a first-order approximation for a perfectly conducting planetary surface with Gaussian roughness statistics by Simpson (1993):

$$P_R = \sigma \frac{P_T G_T G_R \lambda^2}{64\pi^3 |\mathbf{r}|^2 |\mathbf{t}|^2} \tag{26}$$

where P_T is the transmitted power, G_T is the spacecraft antenna gain, G_R is the receiving antenna gain, and σ is the integrated bistatic radar cross section; no atmospheric losses are assumed at this stage.

For a perfectly conducting surface of radius R_p with gently undulating roughness, it is assumed (Fjeldbo, 1964):

$$\sigma = \frac{4\pi |t^2| Rp^2 \cos\phi}{\left(Rp\cos\phi + 2|t'|\right)\left(Rp + 2|t'|\cos\phi\right)} \tag{27}$$

where $\phi = \phi_i + \phi_s$

6.2 Effective scattering area and antenna beam and bandwidth effects

The area of the integrated cross-section for normal incidence ($\phi = \phi_i + \phi_s = 0^o$) is estimated by an 'effective' scattering area A_{eff}. This area can be expressed according to Simpson (1993) as:

$$A_{eff} = \pi r_{eff}^2 \tag{28}$$

Assuming for the surface roughness ξ a value of 0.1 rad, the effective scattering area can be estimated as:

$$r_{eff} \sim \begin{cases} 2R_p\xi & h_r >> R_p \\ 2h_r\xi & h_r << R_p \end{cases} \tag{29}$$

where R_p is the planetary radius and h_r is the vertical height of the spacecraft above the planetary surface. For further analysis, two distances are assumed for conducting a bistatic radar experiment: $h_r \sim 1000$ km and $h_r \sim 15\,000$ km. The effective scattering area A_{eff} and r_{eff} are then given by:

$$r_{eff} \sim 2 \times 10^5 \text{ m}; \; A_{eff} \sim 1.2 \times 10^{11} \text{ m}^2 \tag{30}$$

$$r_{eff} \sim 1.2 \times 10^5 \text{ m}; \; A_{eff} \sim 4.5 \times 10^{12} \text{ m}^2 \tag{31}$$

	S-Band		X-Band	
h_r [km]	1000	15 000	1000	15 000
r_{eff} [m]	2×10^5	1.2×10^6	2×10^5	1.2×10^6
A_i [m^2]	3.4×10^{10}	7.6×10^{12}	2.5×10^9	5.6×10^{11}
A_i / A_{eff}	0.29	1.7	0.02	0.12
v (km/s)	9	4.8	9	4.8
λ [m]	0.13	0.13	0.036	0.036
β (°)	90	90	90	90
θ_{3dB} (°)	6	6	1.6	1.6
B_{obs} (kHz)	14.5	7.7	14.0	7.4
V (km/s)	7.7	1.48	7.7	1.48
B (kHz)	19.7	3.8	71.2	13.7

Table 5. Scattering areas and beam parameters.

The effective scattering area for oblique incidences becomes an ellipse elongated in the spacecraft-Earth direction and h_r should be replaced by the slant range. The details are cumbersome and are not addressed here.

For Venus Express, it is assumed in the following a half-power beam width θ_{3dB} of the HGA reflector antenna: S-band ~6°; X-band ~1.6°. The beam will illuminate the planetary surface within an area A_i. If A_i is smaller than A_{eff}, the power P_{Robs} received at the ground station has to be scaled according to Simpson (1993) by:

$$P_{R_{obs}} \sim P_R \frac{A_i}{A_{eff}} \tag{32}$$

Otherwise ($A_i > A_{eff}$), we can set:

$$P_{Robs} \sim P_R \tag{33}$$

For quasi-specular scattering, the corresponding echo spectrum has a half-power width (Simpson, 1993):

$$B = 4\,(\ln 2)^{1/2}\,(V\xi/\lambda)\cos\phi \tag{34}$$

where V is the velocity of the specular point across the surface.

For finite antenna beam illumination, the Doppler spread B_{obs} is approximately:

$$B_{obs} = \frac{2|v|}{\lambda}\sin\beta\,\sin\theta_{3dB} \tag{35}$$

where β is the angle between the antenna boresight (aimed at the specular point) and the spacecraft velocity **v**. For the two cases of h_r here, the results shown in Table 5 are obtained.

Table 5 shows that the S-band is beam-limited at low altitudes for S-band while the bistatic radar reflection will always be beam-limited at X-band. This means that the received signal strength is reduced owing to the finite illumination

Table 6. Signal-to-noise ratios for a bistatic radar experiment based on a 1 s integration time. Earth-Venus distance 0.8 AU; no atmospheric losses included. DSS-63 or equivalent foreseen as ground station.

	S-Band		*X-Band*	
h_r [km] = $\lvert t' \rvert$	1000	15000	1000	15000
P_T (dBW)	7	7	18.1	18.1
G_T (dB)	25.7	25.7	37.0	37.0
G_R (dB)	63.3	63.3	74.3	74.3
L_s (dB)	-261.3	-261.3	-272.6	-272.6
$\sigma = \frac{4\pi \lvert t \rvert^2 Rp^2}{\left(Rp + 2h_T\right)^2}\left(dbm^2\right)$	128.5	139.00	128.5	139.0
4π *(dB)*	-11	-11	-11	-11
t^2 (dBm^2)	-136.9	-146.5	-136.9	-146.5
Additional system losses (dB)	-3	-3	-3	-3
P_R (dBW)	-187.7	-186.8	-165.6	-164.7
Correction factor A_j/A_{eff} (dB)	-5.4	0	-17	-9.1
P_{Robs} (dBW)	-195.5	-186.8	-182.6	-173.8
B_{obs} (dBHz)	41.6	38.9	41.5	38.7
T_{sys} (dBK)	13.0	13.0	14.0	14.0
k (dBW/Hz K)	-228.6	-228.6	-228.6	-228.6
P_N (dBW)	-174.0	-176.7	-173.1	-175.9
P_{Robs}/P_N (dB)	-21.5	-10.1	-9.5	-2.1
Processing Gain in $\sqrt{B_{obs}}$	20.8	19.4	20.7	19.8
Detectability D (1/s)	-0.7	9.3	11.2	21.9

of the quasi-specular scattering region, which places demands on pointing and timing accuracies. For comparison purposes, α has been approximated in all cases to be 90º and V by the spacecraft velocity projected onto the surface. As before, it is assumed that $\phi = 0$ and $\xi = 0.1$.

6.3 Link budget and signal detectability

With L_s being the free-space loss given by $(4\pi r/\lambda)^2$, t the planetocentric radial distance of the spacecraft and $P_N = kT_{sys}B$ the noise power in the considered bandwidth given either by Eq. 34 or Eq. 35, the values shown in Table 6 are obtained for the received signal-to-noise power ratio P_{Robs}/P_N (dB) and the signal detectability D (1/s). In general, D should be greater than unity. The significance of D ~ 1 measurements can be increased by averaging over time, if the signal's statistical character does not change during the averaging interval (Simpson, 1993).

The atmospheric losses that need to be considered because the radio beam penetrates the absorption layers (twice: before and after reflection from the surface) depend on the geometrical conditions of the experiment. Looking at Fig. 3 and assuming reasonable oblique angles provide estimated loss factors of

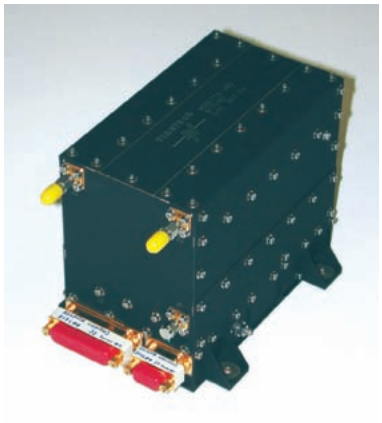

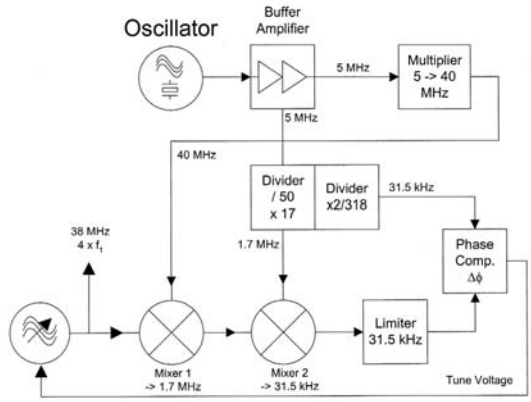

Fig. 14 (left). The Engineering Model of VeRa's USO. The manufacturer is Timetech GmbH.

Fig. 15 (right). The 5–38.2 MHz synthesiser (Pawlitzki & Schwall, 2004).

≤ 3 dB for X-band and < 0.3 dB for S-band. This shows that, at distances close to Earth, bistatic radar experiments can be executed with very promising results when a powerful ground station equivalent to DSS-63 (preferentially DSS-43, in Canberra, Australia) is used. Using NNO would lead, according to Table 2, to a degradation of approximately 10 dB, so it is not planned for even small Earth-Venus distances.

7. Instrumentation

7.1 The Ultrastable Oscillator (USO)

The USO (Fig. 14) provides the reference frequency (38.268500 MHz) for the Venus Express transponder. It is a direct derivative of the qualified and launched Rosetta USO. Its design is based on the unique 'BVA' (boîte vieillage ameliorée) resonator design. The BVA resonator consists of an electrodeless stress compensated-cut, 5 MHz third-overtone crystal resonator, which is decoupled from its mounting structure by four rigid quartz bridges machined from a monolithic block. This design consists of a sandwich of three crystal plates rigidly clamped together. In contrast to conventional designs, the metallisation is deposited on the non-resonating outer two elements; the resonator itself is pure quartz capacitively coupled to the outer electrodes. This design eliminates contamination problems linked to ion migration in the resonator and reduces constraints to the mounting structure.

To achieve the requested frequency, a synthesiser (Fig. 15) is needed. There is no numerically-controlled oscillator and no software or microprocessor in this design. All division and multiplication ratios are fixed by hard-wired design.

The inherent design of the resonator guarantees an ageing rate of $1x10^{-11}$/day after a continuous operation of 30 days. The USO is further characterised by an extreme low phase noise, resulting in an excellent frequency stability (Allan deviation ~3×10^{-13} at 1–100 s). Its dimensions are 16.1 x 13.0 x 13.0 cm and 1.5 kg; power consumption is ~5 W. The radio-frequency output can be muted by a special command while the ultrastable oscillator is still powered.

7.2 The calibration measurements

The calibration measurements performed at the unit, subsystem and system levels verified that the USO-transponder system delivers the radio-frequency signals with adequate qualities of frequency stability, phase noise and group delay. The test method relied on the phase-detector method and the usage of ultrastable quartz oscillators installed as frequency reference sources in the VeRa electrical ground system equipment. The test set-up and results are described in detail in Hagl et al. (2004), Häusler & Remus (2004) and Mattei et al. (2004).

As an example, the phase noise spectrum measured in the one-way mode is

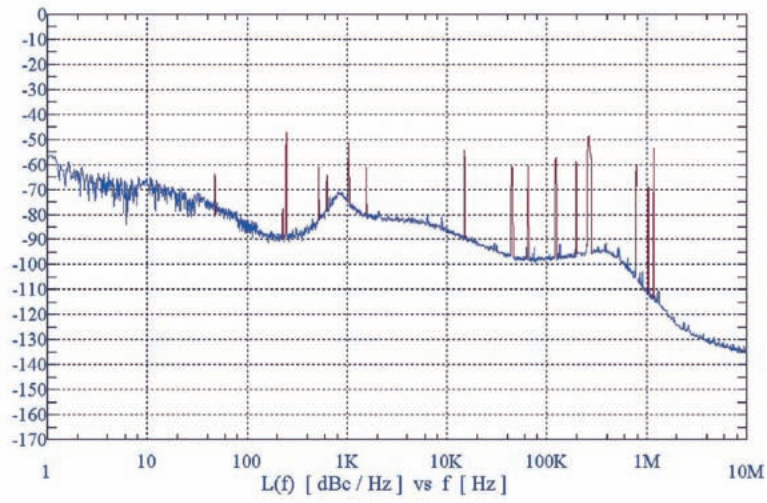

Fig. 16. Phase noise spectrum of USO and transponder 02 in the ONED mode at X-band (Mattei et al., 2004).

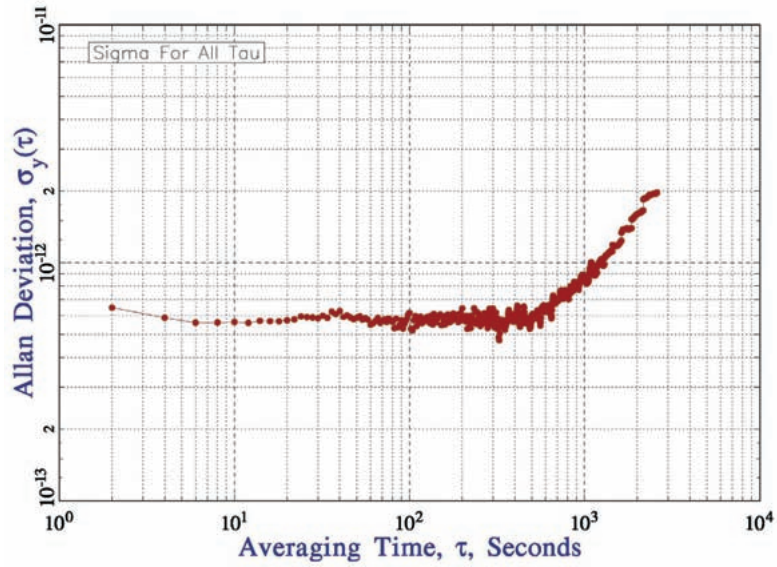

Fig. 17. ONED-X frequency stability of the Fligh Model USO, transponder 02. USO warm-up time ~11 h; frequency values were not corrected for drift effects (Mattei et al., 2004).

shown in Fig. 16. The spectrum shows clean behaviour close to the carrier in the relevant frequency range $f < 50$ Hz without contamination by spurious signals (after elimination of 50 Hz harmonics). At higher frequencies, transponder-spacecraft emissions are present, however, with a negligible total power contribution. It can also be concluded that bistatic radar experiments that investigate the spectral behaviour of the scattered radio signal over a wide frequency range can be successfully conducted with the USO as the reference frequency source in the ONED transmission mode.

The parameter most closely related to the frequency stability of the radio frequency-carrier and the related Doppler noise is the Allan deviation $\sigma_y(\tau)$. For a definition and thorough treatment of oscillator instabilities, see (Rutman, 1978). Fig. 17 shows the result of the Allan deviation measurement performed at the system-level. Owing to the test circumstances, the requested minimum stabilisation time of the USO was never achieved. Based on the results obtained with the VeRa Engineering Qualification Model USO and Flight Model transponder 02 (Häusler & Remus, 2004), plus the Rosetta flight experience (Pätzold, 2004), some improvement in the USO flight performance can be expected.

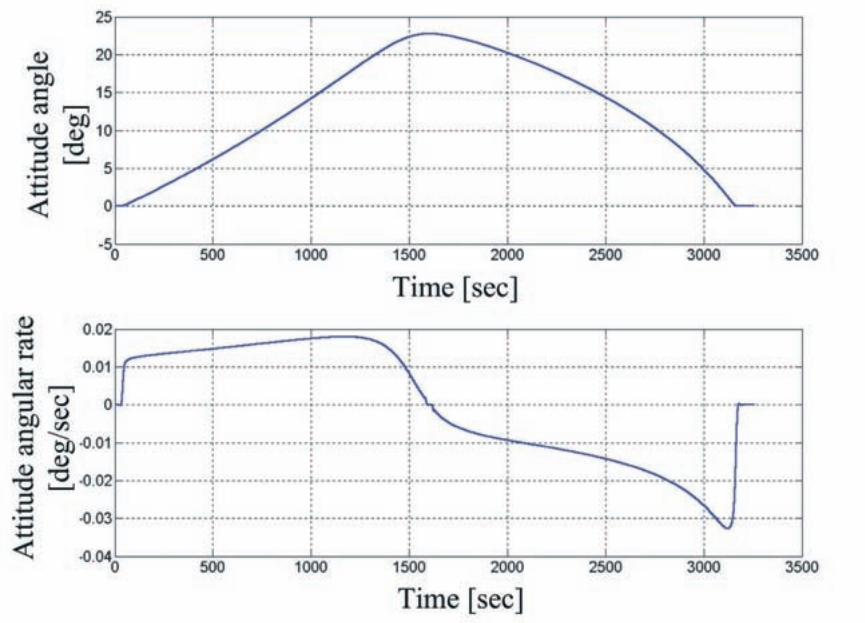

Fig. 18. Venus Express spacecraft attitude correction angle and its time-derivative applied in the near-diametric occultation of orbit 105 (Remus, 2004).

The dense atmosphere of Venus bends the path of microwave rays considerably during atmospheric occultation experiments. Special spacecraft steering is required to compensate for this effect as the occultation geometry changes from ingress to egress (Fig. 18). With no spacecraft steering, the radio energy emitted within the 3 dB antenna opening angle θ_{3dB} from the HGA (~1.6° for X-band) will miss the Earth if the rays deviate from a straight line by more than this angle. For deep occultations, bending angles can amount to ~25°. The requirement for precise spacecraft attitude manoeuvres both in time and space is obvious. VeRa requires an angular uncertainty of less than 0.2 times the opening angle. This ensures that the measured signal power variations linked to atmospheric absorption effects are not misinterpreted as variations in the antenna radiation pattern. Precise steering manoeuvres are also required for the bistatic radar experiments. As discussed in Section 3.6, the precise execution in absolute time is a prerequisite for the success of these experiments. VeRa requires time accuracies of 1 s for the bistatic radar experiments and 5 s for the occultation experiments.

Before each experiment, VeRa issues a set of Chebyshev polynomials specifying the time sequence of quaternions that define the attitude manoeuvre. The details of the attitude predictions are cumbersome; they are thoroughly explained in Häusler et al. (2003). As an example, Fig. 18 shows the variation of the total angle with time and its time derivative during the near-diametric occultation in sample orbit 105.

8. Spacecraft Attitude Manoeuvres

References

Arvidson, R.E., Bracket, R.A., Shepard, M.K., Izenberg, N.R. & Fegley, B. Jr., (1994). Microwave Signatures and Surface Properties of Ovda Regio and Surroundings, Venus. *Icarus* **112**, 171–186.

Astrium (2003). *VEX.AST,CO.0026, Venus Express Partnership Agreement, Issue 2, Rev. 4*, 1 July 2003.

Astrium (2004). *Space/Ground Link Budgets S/X Band, VEX-T. ASTR-TCN-0171, 13.0*, 15 February 2004.

Barriot, J.-P., Vales, N., Balmino, G. & Rosenblatte, P. (1998). A 180th Degree and Order Model of the Venus Gravity Field from Magellan Line of Sight Residual Doppler Data. *J. Geophys. Res. Lett.* **25**, 3743–3746.

Bird, M.K., Volland, H., Pätzold, M., Edenhofer, P., Asmar, S.W. & Brenkle, J.P.

(1994). The Coronal Electron Density Distribution Determined from Dual-Frequency-Frequency Ranging Measurements during the 1991 Solar Conjunction of the Ulysses Spacecraft. *Astrophys. J.* **426**, 373–381.

Bird, M.K., Allison, M., Asmar, S.W., Atkinson, D.H., Edenhofer, P., Heyl, M., Iess, L., Plettemeier, D., Tyler, G.L. & Wohlmuth, R. (1997). The Huygens Doppler Wind Experiment. In *Huygens: Science, Payload and Mission* (Ed. A. Wilson), SP-1177, ESA Publications Division, ESTEC, Noordwijk, The Netherlands, pp139–162.

Borderies, N.J. (1991). JPL InterOffice Memorandum 314.6-1347.

Born, M. & Wolf, E. (1970). *Principles of Optics*, Pergamon Press, London, UK.

Counselman, C.C., III., Gourevitch, R.W., King, R.W. & Loriot, G.B. (1980). Zonal and Meridional Circulation of the Lower Atmosphere of Venus determined by Radio Interferometry. *J. Geophys. Res.* **85**, 8026–8030.

Eshleman, V.R. (1973). The Radio Occultation Method for the Study of Planetary Atmospheres. *Planet. Space Sci.* **21**, 1521–1531.

Eshleman, V.R., Tyler, G.L., Anderson, J.D., Fjeldbo, G., Levy, G.S., Wood, G.E. & Croft, T.A. (1977). Radio Science Investigations with Voyager. *Space Sci. Rev.* **21**(2), 207–232.

Fjeldbo, G. (1964). Bistatic-Radar Methods for Studying Planetary Ionospheres and Surfaces. Ph.D. Thesis, Stanford University, USA.

Fjeldbo, G. & Eshleman V.R. (1969). Atmosphere of Venus as Studied with the Mariner 5 Dual Radio-Frequency Occultation Experiment. *Radio Science* **4**(10), 879–897.

Fjeldbo, G., Kliore, A.J. & Eshleman, R. (1971). The Neutral Atmosphere of Venus as Studied with the Mariner V Radio Occultation Experiments. *Astron. J.* **76**(2), 123.

Ford, P.G. & Pettengill, G.H. (1983). Venus: Global Surface Radio Emissivity. *Science* **220**, 1379–1381.

Gierasch, P.J. (1975). Meridional Circulation and the Maintenance of the Venus Atmospheric Rotation. *J. Atm. Sci.* **32**, 1038–1044.

Hagl, D., Remus, S. & Häusler, B. (2004). USO Phase Noise Performance of EM at 38 MHz & FM at 5 MHz, VEX-VERA-UBW-RP-4100, I1.0, 9 February 2004, Venus Express project documentation, Universität der Bundeswehr München, Germany.

Han, C.S. & Tyler, G.L. (2003). Resolving Diffractive and Guiding Structures in Thick Atmospheres. *Geophys. Res. Abstr.* **5**, 14285.

Häusler, B. (2002). *Radio Science Messungen im Sonnensystem. Mit einer Einführung in die Theorie der Gravitation*. Forschungsbericht Universität der Bundeswehr München, LRT-WE-9-FB-2.

Häusler, B., Eidel, W., Hagl, D., Remus, S., Selle, J. & Pätzold, M. (2003). Venus Express Radio Science Experiment VeRa, Reference Systems and Techniques used for the Simulation and Prediction of Atmospheric and Ionospheric Sounding Measurements at Planet Venus. Forschungsbericht LRT-WE-9-FB-4, Universität der Bundeswehr München, Germany.

Häusler, B. & Remus, S. (2004). VeRa Experiment Integrated Test Report: Flight Model Transponder & Engineering Model USO. VEX-VERA-UBW-TR-4001, I1.0, 9 October 2004, Venus Express project documentation, Universität der Bundeswehr München, Germany.

Häusler, B., Remus, S. & Pätzold, M. (2004a). Radio Science Experiment VeRa-Science Performance Analysis. VEX-VERA-UBW-TN-3006, I.2.3, 18 March 2004, Venus Express project documentation, Universität der Bundeswehr München, Germany.

Häusler, B., Remus, S. & Mattei, R. (2004b). USO FM Performance Test at 38 MHz. VEX-VERA-UBW-RP-4200, I1.2, 12 July 2004, Venus Express project documentation, Universität der Bundeswehr München, Germany.

Hinson, D.P. & Jenkins, J.M. (1995). Magellan Radio Occultation Measurements of Atmospheric Waves on Venus. *Icarus* **114**, 310–327.

Hinson, D.P., Twicken, J.D. & Karayel, E.T. (1998). Jupiter's Ionosphere: New Results from Voyager 2 Radio Occultation Measurements. *J. Geophys. Res.* **103**, 9505–9520.

Howard, H.T., Tyler, G.L., Fjeldbo, G., Kliore, A.J., Levy, G.S., Brunn, D.L., Dickinson, R., Edelson, R.E., Martin, W.L., Postal, R.B., Seidel, B., Sesplaukis, T.T., Shirley, D.L., Stelzried, C.T., Sweetnam, D.N., Zygielbaum, A.J., Esposito, P.B., Anderson, J.D., Shapiro, I.I. & Reasenberg, R.D. (1974). Venus: Mass, Gravity Field, Atmosphere, and Ionosphere as Measured by the Mariner 10 Dual-Frequency Radio System. *Science* **183**, 1297–1301.

Howard, H.T., Eshleman, V.R., Hinson, D.P., Kliore, A.J., Lindal, G.F., Woo, R., Bird, M.K., Volland, H., Edenhofer, P., Pätzold, M. & Porsche, H. (1992). Galileo Radio Science Investigations. *Space Sci. Rev.* **60**, 565–590.

Izakov, M.N. (2001). A Possible Mechanism of Superrotation of the Atmosphere of Venus. *Solar System Res.* **35**(4), 249–260.

Jenkins, J.M. & Steffes, P.G. (1991). Results for 13-cm Absorptivity and H_2SO_4 Abundance Profiles from the Season 10 (1986) Pioneer Venus Orbiter Radio Occultation Experiment. *Icarus* **90**, 129–138.

Jenkins, J.M., Steffes, P.G. & Hinson, D.P., Twicken, J.D. & Tyler, G.L. (1994). Radio Occultation Studies of the Venus Atmosphere with the Magellan Spacecraft, 2. Results from the October 1991 Experiments. *Icarus* **110**, 79–94.

JIVE (2003). VLBI Observations of the Huygens Probe, Assessment Study Report. *JIVE Research Note # 0004*, 10 July 2003, Joint Institute for VLBI in Europe (JIVE), Dwingeloo, The Netherlands.

Karayel, E.T. & Hinson, D.P.. (1997). Sub-Fresnel-Scale Vertical Resolution in Atmospheric Profiles from Radio Occultation. *Radio Science* **32**, 411–423.

Karl, J., Pätzold, M. & Bird, M.K. (1997). Coronal Radio Sounding: Non Gaussian Turbulence in the Source Regions of the Solar Wind. *Geophys. Res. Lett.* **24**, 2881–2884.

Keating, G.M., Taylor, F.W., Nicholson, J.Y. & Hinson, E.W. (1979). Short Term Cyclic Variations and Diurnal Variations in the Venus Upper Atmosphere. *Science* **205**, 62–64.

Kliore, A.J. & Patel, I.R. (1982). Thermal Structure of the Atmosphere of Venus from Pioneer Venus Radio Occultations. *Icarus* **52**, 320–334.

Klose, K.B., Wood, J.A. & Hashimoto, A. (1992). Mineral Equilibria and the High Radar Reflectivity of Venus Mountaintops. *J. Geophys. Res.* **97**, 16353–16369.

Kolodner, M.A. & Steffes, P.G. (1998). The Microwave Absorption and Abundance of Sulfuric Acid Vapor in the Venus Atmosphere Based on New Laboratory Measurements. *Icarus* **132**, 151–169.

Konopliv, A.S., Banerdt, W.B. & Sjogren, W.L. (1999). Venus Gravity: 180th Degree and Order. *Icarus* **139**(1), 3–18.

Kreslavsky, M., Ford, P., Pettengill, G. & Head, J. (2005). New Results from the Magellan Bistatic Radar Experiment: A Prototype for Venus Surface Studies with VeRa. *Geophys. Res. Abstracts* **7**, 05757.

Krisher, T.P. (1993). Parametrized Post-Newtonian Gravitational Redshift. *Phys. Rev. D* **48**(10), 4639–4644.

Lee, S.W. (1996). Magellan V RSS 5 Occultation Profile Ref Temp Pres Dens V1.0. MGN-V-RSS-5-OCC-PROF-RTPD-V1.0 *MG 2401*, NASA Planetary Data System.

Leftwich, T.E., von Frese, R.R.B., Kim, H.R., Potts, L.V., Roman, D.R. & Tan, L. (1999). Crustal Analysis of Venus from Magellan Satellite Observations at Atalanta Planitia, Beta Regio, and Thetis Region. *J. Geophys. Res.* **104**(E4), 8441–8462.

Lipa, B. & Tyler, G.L. (1979). Statistical and Computational Uncertainties in Atmospheric Profiles from Radio Occultation: Mariner 10 at Venus. *Icarus* **39**, 192–208.

Luhmann, J.G. (1986). The Solar Wind Interaction with Venus. *Space Sci. Rev.* **44**, 241–306.

Mahajan, K.K. & Diwivedi, A.K. (2004). Ionospheres of Venus and Mars: A Comparative Study. *Adv. Space Res.* **33**, 145–151.

Mattei, R., Remus, S. & Häusler, B. (2004). VeRa Experiment Integrated Test Report: Flight Mode Transponder & Flight Model USO, VEX-VERA-UBW-TR-4002, I1.1, 17 December 2004, Venus Express project documentation, Universität der Bundeswehr München, Germany.

Moroz, V.I. (2002). Studies of the Atmosphere of Venus by Means of Spacecraft: Solved and Unsolved Problems. *Adv. Space Res.* **29**(2), 215–225.

Newman, M., Schubert, G., Kliore, A.J. & Patel, I.R. (1984). Zonal Winds in the Middle Atmosphere of Venus from Pioneer Venus Radio Occultation Data. *J. Atmos. Sci.* **41**(12), 1901–1913.

Pawlitzki, A. & Schwall, Th. (2004). VeRa USO Detailed Design Document, VE-TIM-DD-3001, I5.0, 12 February 2004, Venus Express project documentation, TimeTech GmbH, Stuttgart, Germany.

Pätzold, M. (2004). Report on NEVP Commissioning Operations March, May, September and October 2004, ROS-RSI-IGM-TR-3117, I2.0, 1 November 2004, Rosetta project documentation, Institute for Geophysics and Meteorology, University of Cologne, Cologne, Germany.

Pätzold, M. & Häusler, B. (2004). VeRa Flight Operations Manual, Experiment User Manual. VEX-VERA-IGM-MA-3005, I2.3, 14 July 2004, Venus Express project documentation, Institute for Geophysics and Meteorology, University of Cologne, Cologne, Germany.

Pätzold, M., Bird, M.K., Edenhofer, P., Asmar, S.W. & McElrath, T.P. (1995). Dual-Frequency Radio Sounding of the Solar Corona during the 1995 Conjunction of the Ulysses Spacecraft. *J. Geophys. Res. Lett.* **22**, 3313–3316.

Pätzold, M., Karl, J. & Bird, M.K. (1996). Coronal Sounding with Ulysses: Phase Scintillation Spectra in Coronal Holes and Streamers. *Astron. Astrophys.* **316**, 449–456.

Pätzold, M., Hausler, M., Aksnes, K., Anderson, J.D., Asmar, S.W., Barriot, J.-P., Bird, M.K., Boehnhardt, H., Eidel, W., Grun, E., Ip, W.H., Marouf, E., Morley, T., Neubauer, F.M., Rickman, H., Thomas, N., Tsurutani, B.T., Wallis, M.K., Wickramasinghe, N.C., Mysen, E., Olson, O., Remus, S., Tellmann, S., Andert, T., Carone, C., Fels, M., Stanzel, C., Audenrieth-Kersten, I., Gahr, A., Muller, A.-L., Stupar, D. & Walter, C. (2006). Rosetta Radio Science Investigations. *Space Sci. Res.*; submitted.

Pätzold, M., Neubauer, F.M., Carone, L., Hagermann, A., Stanzel, C., Häusler, B., Remus, S., Selle, J., Hagl, D., Hinson, D.P., Simpson, R.A., Tyler, G.L., Asmar, S.W., Axford, W.I., Hagfors, T., Barriot, J.-P., Cerisier, J.-C., Imamura, T., Oyama, K.-I., Janle, P., Kirchengast, G. & Dehant, V. (2004). MaRS: Mars Express Orbiter Radio Science. In *Mars Express: The Scientific Payload* (Ed. A. Wilson), SP-1240, ESA Publications Division, Noordwijk, The Netherlands.

Pettengill, G.H., Ford, P.G. & Nozette, S. (1982). Venus: Global Surface Radar Reflectivity. *Science* **217**, 640–642.

Pettengill, G.H., Ford, P.G. & Simpson, R.A. (1996). Electrical Properties of the Venus Surface from Bistatic Radar Observations. *Science* **272**, 1628–1631.

Pettengill, G.H., Ford, P.G. & Wilt, R.J. (1992). Venus Surface Radiothermal Emission as Observed by Magellan. *J. Geophys. Res.* **97**(E8), 13091–13102.

Reasenberg, R.D., Shapiro, I.I., MacNeil, P.E., Goldstein, R.B., Breidenthal, I.C. Brenkle, J.P., Cain, D.L., Kaufman, T.M., Komarek, T.A. & Zygielbaum, A.I. (1979). Viking Relativity Experiment: Verification of Signal Retardation by Solar Gravity. *Astrophys. J.*, **234**, L219.

Remus, S. (2004). *Untersuchungen zur Durchführung von satellitengestützten Radio Science Experimenten im interplanetaren Raum*, PhD thesis, Universität der Bundeswehr München, Neubiberg, Germany, Fakultät für Luft- und Raumfahrttechnik, June 2004.

Robinson, C. & Wood, J. (1993). Recent Volcanic Activity on Venus: Evidence from Radiothermal Emissivity Measurements. *Icarus* **102**, 26–39.

Rodriguez-Canabal, J., Yanez, A. & Sanchez Perez, J.M. (2003). Venus Express: Consolidated Report on Mission Analysis (Issue 1). VEX-ESC-RP-5500, April 2003, Venus Express documentation, ESOC/ESA, Darmstadt, Germany.

Russell, C.T. & Vaisberg, O.L. (1983). The Interaction of the Solar Wind with Venus. In *Venus* (Ed. D.M. Hunton, L. Colin, T.M. Donahue & V.I. Moroz), Univ. of Arizona Press, pp.873–940.

Rutman, J. (1978). Characterization of Phase and Frequency Instabilities in Precision Frequency Sources: Fifteen Years of Progress. *Proc. IEEE* **66**(9), 1048-1075.

Sagdeev, R., Kerzhanovitch, V.V., Kogan, L.R., Kostenko, V.I., Linkin, V.M., Matveyenko,L.I., Nazirov, R.R., Pogrebenko, S.V., Struckov, I.A., Preston, R.A., Purcel, J., Hildebrand, C.E., Grishmanovskiy, V.A., Kozlov, A.N., Molotov, E.P., Blamont, J.E., Boloh, L., Laurans, G., Kaufmann, P., Galt, J., Biraud, F., Boischot, A., Ortega-Molina, A., Rosolem, C., Petit, G., Mezger, P.G., Schwartz, R., Ronnang, B.O., Spencer, R.E., Nicolson, G., Rogers, A.E.E., Cohen, M.H., Martirosyan, R., Moiseyev, I.G. & Jatskiv, J.S. (1992). Differential VLBI Measurements of the Venus Atmosphere Dynamics by Balloons: VEGA Project. *Astron. Astrophys.* **254**, 387–392.

Saunders, R.S. (1997). Venus. In *Encyclopedia of Planetary Sciences* (Eds. J.H. Shirley & R.W. Fairbridge), Chapman & Hall, pp887-889.

Schaefer, L. & Fegley, B., Jr. (2004). Heavy Metal Frost on Venus. *Icarus* **168**(1), 215–219.

Schneider, M. (1996). *Himmelsmechanik, Bd. III, Gravitationstheorie*, Spektrum Verlag, Germany.

Selle, J., Häusler, B. & Pätzold, M. (2004). Planung und Simulation von Radio Science Messungen im Rahmen der interplanetaren Raumfahrt-Missionen Mars Express und Venus Express. In *DGLR-Jahrestagung (Annual Meeting), Conf. Proc.*, DGLR-2004-065, Dresden, Germany.

Shapiro, I.I. (1964). Fourth Test of General Relativity. *Phys. Rev. Lett.*, **13**, 789.

Simpson, R.A. (1993). Spacecraft Studies of Planetary Surfaces using Bistatic Radar. *IEEE Transact. Geosci. Rem. Sens.* **31**(2), 465.

Soffel, M.H. (1989). *Relativity in Astrometry, Celestial Mechanics and Geodesy*, Springer Verlag, Germany.

Sovers, O.J., Fanselow, J.L. & Jacobs, C.S. (1998). Astrometry and Geodesy with Radio Interferometry: Experiments, Models, Results. *Rev. Modern Phys.* **70**(4), 1393–1454.

Steffes, P.G., Jenkins, J.M., Austin, R.S., Asmar, S.W., Lyons, D.T., Seale, E.H. & Tyler, L.G. (1994). Radio Occultation Studies of the Venus Atmosphere with the Magellan Spacecraft, 1. Experimental Description and Performance. *Icarus* **110**, 71–78.

Taylor, F.W. (1997). Venus: Atmosphere. In *Encyclopedia of Planetary Sciences* (Eds. J.H. Shirley & R.W. Fairbridge), Chapman & Hall, pp890-895.

Taylor, F.W. (2002). Some Fundamental Questions Concerning the Circulation of the Atmosphere of Venus. *Adv. Space Res.* **29**(2), 227–231.

Titov, D., Lellouch, E., Taylor, F.W., Marinangeli, L., Opgenoorth, H., Barabash, S., Bertaux, J.-L., Drossart, P., Formisano, V., Hausler, B., Korablev, O., Markiewicz, W.J., Patzold, M., Picardi, G., Piccioni, G., Plaut, J., Sauvaud, J.-A., Simon, P., Lebreton, J.-P., Coradini, M., Whitcomb, G.,

McCoy, D., Koeck, Ch., Kemble, S., Gautret, L., Renard, P. & Faye, F. (2001). Venus Express – An Orbiter for the Study of the Atmosphere, the Plasma Environment, and the Surface of Venus. ESA-SCI (2001) 6, ESA Headquarters, Paris, France, October 2001.

Tyler, G.L. (1987). Radio Propagation Experiments in the Outer Solar System with Voyager. *Proc. IEEE* **75**(10), 1404–1431.

Tyler, G.L., Balmino, G., Hinson, D.P., Sjogren, W.L., Smith, D.E., Asmar, S.M., Priest, P. & Twicken, J.D. (2001). Radio Science Investigation with Mars Global Surveyor: Orbit Insertion through One Year in Mapping Orbit. *Special Issue on Mars Global Surveyor, J. Geophys. Res.* **106**(E10), 23327–23348.

Tyler, G.L., Balmino, G., Hinson, D.P., Sjogren, W.L., Smith, D.E., Woo, R.T., Asmar, S.M., Connally, M.J., Hamilton, C.L. & Simpson, R.A. (1992). Radio Science Investigation with Mars Observer. *J. Geophys. Res.* **97**(E5), 7759–7779.

Tyler, G.L., Ford, P.G., Campbell, D.B., Elachi, Ch., Pettengill, G.H. & Simpson, R.A. (1991). Magellan: Electrical and Physical Properties of Venus' Surface. *Science* **252**, 265–270.

Yakovlev, O.I. (2002). *Space Radio Science*, ESI Book Series, Taylor & Francis, London, UK.

Yamamoto, M. & Takahashi, M. (2003). The Fully Developed Superrotation Simulated by a General Circulation Model of a Venus-like Atmosphere. *J. Atmos. Sci.* **60**, 561–574.

Yuen, J.H. (1983). *Deep Space Telecommunications Engineering,* Plenum Press, New York (USA) and London (UK).

Acknowledgements

The authors are thankful to ESA and EADS-Astrium for supporting the development of the VeRa instrument.